Hindawi
Mathematical Problems in Engineering
Volume 2018, Article ID 6141683, 16 pages
https://doi.org/10.1155/2018/6141683

Research Article

A Stress Approach Model of Moderately Thick, Homogeneous Shells

Axel Fernando Domínguez Alvarado and Alberto Díaz Díaz

Centro de Investigación en Materiales Avanzados, S.C., Miguel de Cervantes 120, Complejo Industrial Chihuahua, 31136 Chihuahua, Chihuahua, Mexico

Correspondence should be addressed to Alberto Díaz Díaz; alberto.diaz@cimav.edu.mx

Received 12 October 2018; Accepted 6 December 2018; Published 31 December 2018

Academic Editor: Francesco Tornabene

Copyright © 2018 Axel Fernando Domínguez Alvarado and Alberto Díaz Díaz. This is an open access article distributed under the Creative Commons Attribution License, which permits unrestricted use, distribution, and reproduction in any medium, provided the original work is properly cited.

This paper presents the theoretical development of a new model of shells called SAM-H (Stress Approach Model of Homogeneous shells) and adapted for linear elastic shells, from thin to moderately thick ones. The model starts from an original stress polynomial approximation which involves the generalized forces and verifies the 3D equilibrium equations and the stress boundary conditions at the faces of the shell. Hellinger-Reissner functional and Reissner's variational method are applied to determine the generalized fields and equations. The generalized forces and displacements are the same as those obtained in a classical, moderately thick shell model (CS model). The equilibrium and constitutive equations have some differences from those of a CS model, mainly in consideration of applied stress vectors at the upper and lower faces of the shell and the stiffness matrices. Another feature of the SAM-H model is the inclusion of the Poisson's effect of out-of-plane normal stresses on in-plane strains. As a first application example to test the accuracy of the model, the case of a pressurized hollow sphere is considered. The analytical results of stresses and displacements of the SAM-H and CS models are compared to those of an exact 3D resolution. In this example, SAM-H model proves to be much more accurate than the CS model and its approximation of the normal out-of-plane stress is very precise. Finally, an implementation of the SAM-H model equations in a finite element software is performed and a case study is analyzed to show the advantages of using the SAM-H model.

1. Introduction

In structural engineering, models of plates and shells are necessary for carrying out reliable predictions of displacements and stresses without the excessive computational cost of three-dimensional solid finite element calculations. Displacement and stress approaches are commonly used as starting point for the construction of these models. In a displacement approach, the displacement field is approximated by linear combinations of friendly functions of the thickness coordinate such as polynomials. In a stress approach, an analogue approximation is made with the components of the 3D stress field. Additionally, in this last approach it is ideal that the approximate stress field verifies the 3D equilibrium equation and stress boundary conditions [1].

In the family of linear elastic plate models, the Kirchhoff-Love theory [2] is the simplest one. In this theory, the plate thickness does not change during deformation and the in-plane displacements are approximated by first degree polynomials of the thickness coordinate while the out-of-plane displacement is uniform across the thickness. The coefficients of these polynomials depend only on the three displacements of the middle surface and their derivatives (these displacements can also be called generalized displacements). This model neglects out-of-plane shear forces and is usually applied to thin plates. A more complete plate model is Mindlin's one [3] which considers the same polynomial degrees in the displacement approximation but includes two rotations in the coefficients of the in-plane displacement polynomials. Five generalized displacements are then involved in Mindlin's model (three displacements and two rotations) and the linear out-of-plane strain remains zero as in Kirchhoff-Love theory. Another model of plates is Reissner's model [4] which is based on a stress approach: the in-plane stresses are approximated

by first degree polynomials while the out-of-plane shear and normal stresses are approximated by second degree and third degree polynomials, respectively. The stress approximation verifies the 3D equilibrium equation and the stress boundary conditions at the upper and lower faces of the plate. The coefficients of the stress polynomials are the stress resultants also called generalized forces. Owing to the shear correction factor introduced by Mindlin, the models of Reissner and Mindlin have similar plate equations: this explains the common denomination "Reissner-Mindlin" plate theory. These models provide accurate stiffness predictions of moderately thick plates and good but less precise results for thick shells. These models have been the starting point for the analysis of composite laminated plates and the development of other models such as higher-order models [5], zig-zag models [6], extensions of Reissner-Mindlin-like models [7, 8], and layerwise models [9]. In this last family of models, Pagano's model [1], which proposes a polynomial stress approximation that verifies the 3D equilibrium in each layer, is worth citing. Pagano used Reissner's variational mixed formulation [10] to build the model. No displacement approximation is made despite the use of a mixed formulation. The Hellinger-Reissner functional and the stress approximation helps to identify 2D generalized displacements. More recent developments of Pagano's approach can be found in [11–13], where some simplifications are adopted to obtain more operational layerwise models. In [13], Alvarez-Lima et al. enhanced a layerwise model called M4-5N (originally developed by Chabot in [11]) in order to include the Poisson's effect of out-of-plane normal stresses on in-plane strains which may have an important impact on plasticity and failure mechanisms. Most models of plates do not take into account this effect.

Shell models can be classified depending on how the ratio η between the thickness to the smallest principal radius is considered in the model equations: thin and moderately thick shell models neglect any term multiplied by η^k for $k \geq 1$ and $k \geq 2$, respectively; thick shell models consider higher-degree terms. The simplest thin shell models are Love's first approximation theories [2, 14–17] which neglect transverse shear deformation and are based on a displacement approach similar to that in Kirchhoff-Love plate theory. Other thin and moderately thick shell models apply a displacement approximation (in the curvilinear coordinate system) analogue to Mindlin's plate model [18, 19]; for example, in [20], Toorani and Lakis proposed a generalization of the classical Reissner-Mindlin plate theory in order to include the curvature and transverse shear strains of the shell. These authors improved their model in [21] by enhancing the kinematic fields. In these displacement approach models, the 3D constitutive equations yield linear in-plane stresses and constant out-of-plane shear stresses across the thickness of the shell. For these models, the stress field does not verify the 3D equilibrium equations and the stress boundary conditions at the faces of the shell [22]. Moreover, the normal out-of-plane stresses and the linear out-of-plane strains are neglected and this may lead to important errors in thicker shells. These drawbacks have motivated the development of higher-degree displacement approximations, the use of better techniques to recover the 3D stress, and the construction of models based on stress or mixed stress/displacement approximations. In [23, 24], Tornabene and Viola used an approximation of the 3D displacement field to obtain all the generalized equations and generalized fields for shells of revolution. After solving the static problem, they applied the generalized differential quadrature method in order to approximate the spatial derivatives of the stress field. This approximation and Hooke's law allowed recovering and correcting the 3D stress field which took into account the boundary conditions at the faces of the shell. One of the first stress approach models for shells is the one developed by Trefftz [25]; in this model, an approximation of in-plane stresses in terms of generalized forces is made, but transverse stresses are neglected. This implies that both 3D equilibrium equations and boundary conditions at the faces of the shell are not verified. In [26, 27], Synge and Chien proposed a mixed stress/displacement approach model for thin shells where stresses and displacements are approximated by polynomials of the thickness coordinate. In their theory, the boundary conditions at the faces of the shell are not fulfilled. In [28], Fang et al. developed a thick shell model using a mixed stress/displacement approach by applying Hellinger-Reissner functional [10]. In this mixed model, the stress field verifies the boundary conditions at the faces of the shell but not the 3D equilibrium equations. Shell models based on a pure stress approach are less usual than those based on a displacement approach; two noteworthy stress approach based models for cylindrical and spherical thick shells can be found in [29, 30], respectively. A summary and comparative study of several shell and plate theories was made by Leissa in [31, 32]. In Leissa's work, all the shell models start with an approximation of the displacement field. There are few models based on a stress approach although these types of models have advantages over those based on displacement approximation.

Many commercial finite element software packages offer surface elements to analyze shell structures. These elements are based on classical shell models. A family of these surface elements is the one introduced in the MITC (Mixed Interpolation of Tensorial Components) shell concept; this family is referred to in the literature as MITC*n*, where *n* is related to the number of nodes in the element [33]. Lee and Bathe [34] state that these elements development is based on the use of displacement interpolations and the selection of appropriate strain field interpolation. Finally, the element rigidity matrix is built using a stress-strain constitutive equation of classical shell models. Obviously, with this family of elements, the stress field does not verify the 3D equilibrium equations and the stress boundary conditions at the faces of the shell.

In this paper, an original model of linear elastic moderately thick shells ($\eta \leq 0.3$) called SAM-H (Stress Approach Model of Homogeneous shells) is developed by making use of a method similar to that applied by Pagano in [1] and based on a stress approach which, in the limit case of a homogeneous plate, involves less generalized forces than Pagano's model. Reissner's variational mixed formulation [10] is applied to obtain the generalized fields and equations. The main contribution of the paper resides on the quality of the

stress approximation and the simplicity of the model: the 3D equilibrium equations and the stress boundary conditions at the shell faces are verified, with the same number of generalized forces, moments, strains, and displacements as the linear elastic version of the classical model of general moderately thick shells proposed by Reddy [19]. Another originality of the model resides on taking into account and distinguishing the effect of stress vectors applied at the inner and outer faces of the shell. Finally, the inclusion of the Poisson's effect of out-of-plane normal stresses on in-plane strains is another feature of the model that has not been found on any thin or moderately thick shell model.

This paper is organized in six sections. In the first section, the adopted notations and assumptions are detailed. The second section recalls the Hellinger-Reissner variational principle of elastostatics. Then, in section three, the proposed stress approximation is shown. The generalized displacements, strains, equilibrium equations, and force edge conditions are obtained in section four. The generalized constitutive equations and displacement edge conditions are determined in section five. In the last section, the main differences between the SAM-H model and a classical shell model are discussed; a comparison of analytical and numerical results of these two models is also shown. Finally, an appendix containing further details of equations is included.

2. Notations, Geometry Definition, and Assumptions

A doubly curved shell is considered. Its thickness h is uniform. (ξ_1, ξ_2, ξ_3) denote the orthogonal curvilinear coordinates where ξ_1 and ξ_2 are the lines of curvature at the middle surface ($\xi_3 = 0$). The principal radii of curvature are R_1 and R_2; the principal curvatures are then $\kappa_1 = 1/R_1$ and $\kappa_2 = 1/R_2$. The Lamé coefficients are defined by

$$A_1 = a_1\left(1 + \frac{\xi_3}{R_1}\right),$$
$$A_2 = a_2\left(1 + \frac{\xi_3}{R_2}\right), \tag{1}$$
$$A_3 = 1$$

where $a_1 = \sqrt{g_{11}^2}$, $a_2 = \sqrt{g_{22}^2}$; $g_{\alpha\beta}$ $(\alpha, \beta = 1, 2)$ are the surface metric tensor components. In what follows, the next notations are adopted:

(i) Greek subscripts take the values 1 and 2;

(ii) Latin subscripts take the values 1, 2, and 3;

(iii) the shell lies in the volume Ω; its middle surface is ω;

(iv) bold face characters denote vectors, matrices, and tensors;

(v) unit vectors in the directions of the lines of curvature are $\mathbf{e_1}$ and $\mathbf{e_2}$; the unit vector normal to the middle surface is $\mathbf{e_3} = \mathbf{e_1} \times \mathbf{e_2}$, where $\times$ is the cross product;

(vi) the dot product of vectors and simple contraction of tensors is noted "$\cdot$" while the double contraction of tensors and the tensor product are noted ":" and "$\otimes$", respectively;

(vii) an underline and a double underline below a bold face character (for example: $\underline{\mathbf{U}}$ and $\underline{\underline{\mathbf{M}}}$) denote, respectively, vectors and second-order tensors of the 2D space defined by the basis $(\mathbf{e_1}, \mathbf{e_2})$;

(viii) $\underline{\underline{\boldsymbol{\kappa}}} = \kappa_1 \mathbf{e_1} \otimes \mathbf{e_1} + \kappa_2 \mathbf{e_2} \otimes \mathbf{e_2}$ and $\underline{\underline{\boldsymbol{\kappa}}}' = \kappa_2 \mathbf{e_1} \otimes \mathbf{e_1} + \kappa_1 \mathbf{e_2} \otimes \mathbf{e_2}$ are curvature tensors;

(ix) the stress vectors applied on the outer ($\xi_3 = h/2$) and inner ($\xi_3 = -h/2$) faces are $\mathbf{s}^+$ and $\mathbf{s}^-$, respectively; these vectors are defined by

$$\mathbf{s}^+(\xi_1, \xi_2) = \underline{\boldsymbol{\tau}}^+ + \sigma^+ \mathbf{e_3}$$
$$\text{and } \mathbf{s}^-(\xi_1, \xi_2) = \underline{\boldsymbol{\tau}}^- + \sigma^- \mathbf{e_3}, \tag{2}$$
$$\text{where } \underline{\boldsymbol{\tau}}^+ = \tau_1^+ \mathbf{e_1} + \tau_2^+ \mathbf{e_2} \text{ and } \underline{\boldsymbol{\tau}}^- = \tau_1^- \mathbf{e_1} + \tau_2^- \mathbf{e_2};$$

in the above expression σ^+ and σ^- are the applied normal stresses while τ_α^+ and τ_α^- are the applied shear stresses.

(x) $\mathbf{f}$ is the 3D body load vector and its components in the curvilinear coordinate system are f_i;

(xi) $\underline{\mathbf{n}}^0 = n_1^0 \mathbf{e_1} + n_2^0 \mathbf{e_2}$ is the outward-pointing normal vector to the edge of the middle surface ω;

(xii) $\boldsymbol{\sigma}$ and $\mathbf{u}$ denote the 3D stress tensor and displacement field;

(xiii) $\mathbf{div}\,\boldsymbol{\sigma}$ denotes the 3D divergence operator applied to the second-order tensor $\boldsymbol{\sigma}$:

$$\mathbf{div}\,\boldsymbol{\sigma} = \frac{1}{A_1 A_2 A_3}\left(\mathbf{v^1} + \mathbf{v^2}\right) \tag{3}$$

where vectors $\mathbf{v^1}$ and $\mathbf{v^2}$ take the array form:

$$\mathbf{v^1} = \begin{pmatrix} \dfrac{\partial A_2 A_3 \sigma_{11}}{\partial \xi_1} + \dfrac{\partial A_1 A_3 \sigma_{12}}{\partial \xi_2} + \dfrac{\partial A_1 A_2 \sigma_{13}}{\partial \xi_3} \\ \dfrac{\partial A_2 A_3 \sigma_{21}}{\partial \xi_1} + \dfrac{\partial A_1 A_3 \sigma_{22}}{\partial \xi_2} + \dfrac{\partial A_1 A_2 \sigma_{23}}{\partial \xi_3} \\ \dfrac{\partial A_2 A_3 \sigma_{31}}{\partial \xi_1} + \dfrac{\partial A_1 A_3 \sigma_{32}}{\partial \xi_2} + \dfrac{\partial A_1 A_2 \sigma_{33}}{\partial \xi_3} \end{pmatrix} \tag{4}$$

and

$$\mathbf{v^2} = \begin{pmatrix} \dfrac{A_2}{a_2}\dfrac{\partial a_1}{\partial \xi_2}\sigma_{21} - \dfrac{A_1}{a_1}\dfrac{\partial a_2}{\partial \xi_1}\sigma_{22} + A_2\dfrac{a_1}{R_1}\sigma_{31} \\ \dfrac{A_1}{a_1}\dfrac{\partial a_2}{\partial \xi_1}\sigma_{12} - \dfrac{A_2}{a_2}\dfrac{\partial a_1}{\partial \xi_2}\sigma_{11} + A_1\dfrac{a_2}{R_2}\sigma_{32} \\ -A_2\dfrac{a_1}{R_1}\sigma_{11} - A_1\dfrac{a_2}{R_2}\sigma_{22} \end{pmatrix}; \tag{5}$$

(xiv) $\underline{\underline{\mathbf{grad}}}\ \underline{\mathbf{g}}$ is the 2D gradient of the 2D vector $\underline{\mathbf{g}} = g_1 \mathbf{e_1} + g_2 \mathbf{e_2}$; its components take the following array form:

$$\underline{\underline{\mathbf{grad}}}\ \underline{\mathbf{g}} = \begin{pmatrix} \dfrac{1}{a_1}\dfrac{\partial g_1}{\partial \xi_1} + \dfrac{g_2}{a_1 a_2}\dfrac{\partial a_1}{\partial \xi_2} & \dfrac{1}{a_2}\dfrac{\partial g_1}{\partial \xi_2} - \dfrac{g_2}{a_1 a_2}\dfrac{\partial a_2}{\partial \xi_1} \\ \dfrac{1}{a_1}\dfrac{\partial g_2}{\partial \xi_1} - \dfrac{g_1}{a_1 a_2}\dfrac{\partial a_1}{\partial \xi_2} & \dfrac{1}{a_2}\dfrac{\partial g_2}{\partial \xi_2} + \dfrac{g_1}{a_1 a_2}\dfrac{\partial a_2}{\partial \xi_1} \end{pmatrix}; \tag{6}$$

(xv) $\underline{\mathbf{grad}}\ p = (1/a_1)(\partial p/\partial \xi_1)\mathbf{e_1} + (1/a_2)(\partial p/\partial \xi_2)\mathbf{e_2}$ is the 2D gradient of the 2D scalar function p;

(xvi) $\underline{\mathbf{div}}\ \underline{\underline{\mathbf{M}}}$ is the divergence of the 2D second-order tensor $\underline{\underline{\mathbf{M}}} = M_{\alpha\beta}\mathbf{e_\alpha} \otimes \mathbf{e_\beta}$ (sum on α and β); its components have the following array form:

$$\underline{\mathbf{div}}\ \underline{\underline{\mathbf{M}}} = \frac{1}{a_1 a_2} \cdot \begin{pmatrix} \dfrac{\partial a_2 M_{11}}{\partial \xi_1} + \dfrac{\partial a_1 M_{12}}{\partial \xi_2} + M_{21}\dfrac{\partial a_1}{\partial \xi_2} - M_{22}\dfrac{\partial a_2}{\partial \xi_1} \\ \dfrac{\partial a_2 M_{21}}{\partial \xi_1} + \dfrac{\partial a_1 M_{22}}{\partial \xi_2} + M_{12}\dfrac{\partial a_2}{\partial \xi_1} - M_{11}\dfrac{\partial a_1}{\partial \xi_2} \end{pmatrix}; \tag{7}$$

(xvii) the divergence of the 2D vector field $\underline{\mathbf{v}} = v_1\mathbf{e_1} + v_2\mathbf{e_2}$ is defined by

$$\operatorname{div} \underline{\mathbf{v}} = \frac{1}{a_1 a_2}\left(\frac{\partial a_2 v_1}{\partial \xi_1} + \frac{\partial a_1 v_2}{\partial \xi_2}\right). \tag{8}$$

The following assumptions are adopted:

(1) small displacements and strains are assumed;

(2) the material is homogeneous and orthotropic, and one of its orthotropy directions is direction 3; $\mathbf{S}$ is the 3D, 4th-order compliance tensor, and its components are S_{ijkl}; while handling plates and shells, it is useful to define the following compliance tensors and constants:

$$\begin{aligned} \underline{\underline{\underline{\underline{\mathbf{S}}}}} &= \sum_{\alpha,\beta,\gamma,\delta=1}^{2} S_{\alpha\beta\gamma\delta}\mathbf{e_\alpha} \otimes \mathbf{e_\beta} \otimes \mathbf{e_\gamma} \otimes \mathbf{e_\delta}, \\ \underline{\underline{\mathbf{S^c}}} &= 2\sum_{\alpha,\beta=1}^{2} S_{\alpha\beta 33}\mathbf{e_\alpha} \otimes \mathbf{e_\beta}, \\ \underline{\underline{\mathbf{S^Q}}} &= 4\sum_{\alpha,\beta=1}^{2} S_{\alpha 3\beta 3}\mathbf{e_\alpha} \otimes \mathbf{e_\beta} \end{aligned} \tag{9}$$

and $S^\sigma = S_{3333}$;

(3) in all calculations the terms ξ_3/R_α and h/R_α are considered, but higher-order terms $(\xi_3/R_\alpha)^n$ and $(h/R_\alpha)^n$ $(n \geq 2)$ are neglected;

(4) the curvatures vary smoothly along the lines of curvature and their derivatives with respect to ξ_α are neglected;

(5) in order to ease the generalized compliance calculations, the divergence of the shear stress vectors applied on the faces of the shell are assumed to be zero:

$$\operatorname{div} \underline{\boldsymbol{\tau}}^+ = \operatorname{div} \underline{\boldsymbol{\tau}}^- = 0; \tag{10}$$

(6) the body load vector $\mathbf{f}$ is uniform through the thickness direction;

(7) no 3D displacement constraints are applied on the inner and outer faces of the shell.

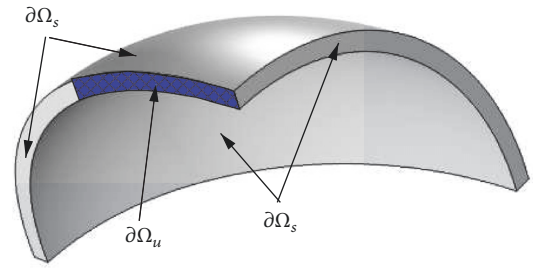

Figure 1: Example of a shell with different regions of boundary conditions.

3. Hellinger-Reissner Functional

On the boundaries $\partial\Omega_\mathbf{u}$ and $\partial\Omega_\mathbf{s}$ of Ω, the body is subjected to the displacement vector $\mathbf{u^g}$ and stress vector $\mathbf{s^g}$, respectively. In Figure 1, an example of the boundaries $\partial\Omega_\mathbf{u}$ and $\partial\Omega_\mathbf{s}$ is shown. The Hellinger-Reissner functional for elastic problems [10] applied to the shell is

$$\begin{aligned} H.R.(\mathbf{u}^*, \boldsymbol{\sigma}^*) = &\int_\Omega \left[\boldsymbol{\sigma}^* : \boldsymbol{\varepsilon}(\mathbf{u}^*) - \mathbf{f}\cdot\mathbf{u}^* - w_e^*\right] d\Omega \\ &- \int_{\partial\Omega_\mathbf{u}} (\boldsymbol{\sigma}^*\cdot\mathbf{n})\cdot(\mathbf{u}^* - \mathbf{u^g})\, dS \\ &- \int_{\partial\Omega_\mathbf{s}} \mathbf{s^g}\cdot\mathbf{u}^* dS \end{aligned} \tag{11}$$

where $\mathbf{n}$ is the 3D outward-pointing normal vector to the boundary of Ω, $\mathbf{u}^*$ is a piecewise C1 first order tensor field, $\boldsymbol{\sigma}^*$ is a piecewise C1 second-order symmetric tensor field, $\boldsymbol{\varepsilon}$ is the Cauchy's infinitesimal strain tensor, and $w_e^* = (1/2)\boldsymbol{\sigma}^* : \mathbf{S} : \boldsymbol{\sigma}^*$ is the elastic energy density. In what follows, a field with an uppercase $*$ denotes a field that is not necessarily the solution of the problem and varies in its corresponding space. If a field (stress, generalized displacement, force, or moment) appears without uppercase $*$, this field is solution of the problem.

In this paper, as in [35], an integration by parts is performed for the term containing $\boldsymbol{\sigma}^* : \boldsymbol{\varepsilon}(\mathbf{u}^*)$.

$$\begin{aligned} H.R.(\mathbf{u}^*, \boldsymbol{\sigma}^*) = &-\int_\Omega \left[\mathbf{div}\,\boldsymbol{\sigma}^*\cdot\mathbf{u}^* + \mathbf{f}\cdot\mathbf{u}^* + w_e\right] d\Omega \\ &+ \int_{\partial\Omega_\mathbf{u}} (\boldsymbol{\sigma}^*\cdot\mathbf{n})\cdot\mathbf{u^g} dS \\ &+ \int_{\partial\Omega_\mathbf{s}} (\boldsymbol{\sigma}^*\cdot\mathbf{n} - \mathbf{s^g})\cdot\mathbf{u}^* dS \end{aligned} \tag{12}$$

Reissner's theorem [10] states that:

(i) the solution to the mechanical problem is the 3D displacement field/stress tensor field couple $(\mathbf{u}, \boldsymbol{\sigma})$ that makes the H.R. functional stationary (notice that no uppercase $*$ appears for the solution);

(ii) the stationarity of H.R. with respect to $\mathbf{u}^*$ yields the equilibrium equations and the boundary conditions on the stress vector while its stationarity with respect to $\boldsymbol{\sigma}^*$ yields the constitutive equations and the boundary conditions on the displacement field.

In this paper, a stress approach is proposed. The introduction of the stress approximation in the H.R. functional in (12) allows identifying the generalized displacements in the thickness integral of the term $\mathbf{div}\,\boldsymbol{\sigma}^* \cdot \mathbf{u}^*$. The stress approximation will lead to 5 generalized displacements (3 displacements and 2 rotations).

4. Stress Approximation

4.1. Polynomial Expressions. Let us define the following polynomial basis of 5-th degree ξ_3-polynomials:

$$\begin{aligned} P_0(\xi_3) &= 1, \\ P_1(\xi_3) &= \frac{\xi_3}{h}, \\ P_2(\xi_3) &= -6\left(\frac{\xi_3}{h}\right)^2 + \frac{1}{2}, \\ P_3(\xi_3) &= -2\left(\frac{\xi_3}{h}\right)^3 + \frac{3}{10}\left(\frac{\xi_3}{h}\right), \\ P_4(\xi_3) &= -\frac{14}{3}\left(\frac{\xi_3}{h}\right)^4 + \left(\frac{\xi_3}{h}\right)^2 - \frac{1}{40} \\ \text{and } P_5(\xi_3) &= \left(\frac{\xi_3}{h}\right)^5 - \frac{5}{18}\left(\frac{\xi_3}{h}\right)^3 + \frac{5}{336}\left(\frac{\xi_3}{h}\right). \end{aligned} \tag{13}$$

This polynomial basis is orthogonal:

$$\int_{-h/2}^{h/2} P_m(\xi_3)\, P_n(\xi_3)\, d\xi_3 = 0 \quad \text{if } m \neq n. \tag{14}$$

The following stress approximations are selected:

$$\sigma^*_{\alpha\beta}(\xi_1,\xi_2,\xi_3) = \sum_{n=0}^{1} \sigma^{n*}_{\alpha\beta}(\xi_1,\xi_2)\, P_n(\xi_3) \tag{15}$$

$$\sigma^*_{\alpha 3}(\xi_1,\xi_2,\xi_3) = \sum_{n=0}^{3} \sigma^{n*}_{\alpha 3}(\xi_1,\xi_2)\, P_n(\xi_3) \tag{16}$$

$$\sigma^*_{33}(\xi_1,\xi_2,\xi_3) = \sum_{n=0}^{4} \sigma^{n*}_{33}(\xi_1,\xi_2)\, P_n(\xi_3) \tag{17}$$

where σ^{n*}_{ij} are stress coefficients which will be expressed as linear combinations of the generalized forces. The polynomial degree of each stress component was chosen so as to verify the 3D equilibrium equation as will be shown in Section 4.3.

4.2. Generalized Forces. Let us define the components of the membrane forces $\underline{\underline{\mathbf{N}}}^*$, shear forces $\underline{\mathbf{Q}}^*$, and moments $\underline{\underline{\mathbf{M}}}^*$ as follows:

$$N^*_{\alpha\beta} = \int_{-h/2}^{h/2} \sigma^*_{\alpha\beta}\left(1 + \frac{\xi_3}{R_{3-\beta}}\right) d\xi_3 \tag{18}$$

$$Q^*_{\alpha} = \int_{-h/2}^{h/2} \sigma^*_{\alpha 3}\left(1 + \frac{\xi_3}{R_{3-\alpha}}\right) d\xi_3 \tag{19}$$

$$M^*_{\alpha\beta} = \int_{-h/2}^{h/2} \xi_3 \sigma^*_{\alpha\beta}\left(1 + \frac{\xi_3}{R_{3-\beta}}\right) d\xi_3 \tag{20}$$

where the subscript $3-\beta$ is 2 if $\beta = 1$, and 1 if $\beta = 2$. The same can be said for the subscript $3-\alpha$. Let us point out that $\underline{\underline{\mathbf{N}}}^*$ and $\underline{\underline{\mathbf{M}}}^*$ may be nonsymmetric, while the stress tensor is always symmetric. Owing to assumption (3) and to the symmetry of the 3D stress tensor, N_{21} and M_{21} are related to N_{12} and M_{12} as follows:

$$\begin{aligned} N_{21} &= N_{12} + \delta\kappa M_{12} \\ \text{and } M_{21} &= \frac{h^2}{12}\delta\kappa N_{12} + M_{12}. \end{aligned} \tag{21}$$

Here $\delta\kappa = \kappa_2 - \kappa_1$. By making use of assumption (3) in Section 2 and introducing the stress approximation defined in (15) and (16), one obtains the following.

$$N^*_{\alpha\beta} = h\sigma^{0*}_{\alpha\beta} + \frac{h^2}{12R_{3-\beta}}\sigma^{1*}_{\alpha\beta} \tag{22}$$

$$Q^*_{\alpha} = h\sigma^{0*}_{\alpha 3} + \frac{h^2}{12R_{3-\alpha}}\sigma^{1*}_{\alpha 3} \tag{23}$$

$$M^*_{\alpha\beta} = \frac{h^3}{12R_{3-\beta}}\sigma^{0*}_{\alpha\beta} + \frac{h^2}{12}\sigma^{1*}_{\alpha\beta} \tag{24}$$

In the limit case of a plate, $\underline{\underline{\mathbf{N}}}^*$ and $\underline{\underline{\mathbf{M}}}^*$ are symmetric and thus the model contains 8 generalized forces and moments, 2 less than Pagano's model [1] applied to a homogeneous plate. The generalized forces and moments of SAM-H are the same as those in the Reissner-Mindlin plate theory.

4.3. Determination of Coefficients in the Stress Approximation. Owing to (3), the 3D equilibrium equation yields the following.

$$\mathbf{v^1} + \mathbf{v^2} + A_1 A_2 \mathbf{f} = \mathbf{0} \tag{25}$$

Introducing (4)-(5) and (15)–(17) in (25) yields

$$\begin{pmatrix} \sum_{q=0}^{2} \eta_1^q(\xi_1,\xi_2)\, P_q(\xi_3) + \sum_{q=0}^{4} \lambda_1^q(\xi_1,\xi_2)\, P_q(\xi_3) + rf_1(\xi_1,\xi_2) \\ \sum_{q=0}^{2} \eta_2^q(\xi_1,\xi_2)\, P_q(\xi_3) + \sum_{q=0}^{4} \lambda_2^q(\xi_1,\xi_2)\, P_q(\xi_3) + rf_2(\xi_1,\xi_2) \\ \sum_{q=0}^{3} \eta_3^q(\xi_1,\xi_2)\, P_q(\xi_3) + \sum_{q=0}^{5} \lambda_3^q(\xi_1,\xi_2)\, P_q(\xi_3) + rf_3(\xi_1,\xi_2) \end{pmatrix} = \begin{pmatrix} 0 \\ 0 \\ 0 \end{pmatrix} \tag{26}$$

where $r = a_1a_2(1 + \xi_3(\kappa_1 + \kappa_2))$ (the terms in $(\kappa_\alpha\xi_3)^2$ are neglected owing to assumption (3) in Section 2) and η_i^q are nonnegligible linear combinations of the stress coefficients σ_{ij}^{n*} and their derivatives with respect to ξ_1 and ξ_2 (none of the terms in η_i^q are multiples of $(\kappa_\alpha h)^2$). The terms λ_i^q are also a linear combination of the stress coefficients but they are neglected because they are multiples of $(\kappa_\alpha h)^2$. By making use of the linear independence of polynomials P_q, the values of the stress coefficients are selected so as to obtain

(i) $\eta_\alpha^2 = 0$; this is ensured by selecting $\sigma_{\alpha 3}^{3*}$ judiciously; in this manner, as mentioned at the end of Section 3, the terms η_α^0 and η_α^1 will provide two generalized equilibrium equations and two generalized displacements for each α value;

(ii) $\eta_3^1 = -a_1a_2h(\kappa_1 + \kappa_2)f_3$ (in order to obtain $\eta_3^1P_1 + rf_3 = 0$), $\eta_3^2 = 0$, and $\eta_3^3 = 0$; this is ensured by a suitable selection of the values of σ_{33}^{2*}, σ_{33}^{3*}, and σ_{33}^{4*}; in this manner, the term in η_3^0 will yield one more generalized equilibrium equation and another generalized displacement.

Owing to (22)–(24), assumptions (3) and (4) in Section 2, and the definition of the stress vectors applied at the inner and outer faces, the obtained stress coefficients σ_{ij}^{n*} are expressed in terms of the generalized forces and applied shear and normal stresses at the faces of the shell. In (A.1)–(A.3) in Appendix A, B, and C, the expression of these stress coefficients is shown. Let us point out that, with these stress coefficients, the 3D boundary conditions at the faces of the shell are verified:

$$\begin{aligned}
&\forall (\xi_1, \xi_2) \in \omega :\\
&\tau_\alpha^+(\xi_1, \xi_2) = \sigma_{\alpha 3}\left(\xi_1, \xi_2, \frac{h}{2}\right),\\
&\tau_\alpha^-(\xi_1, \xi_2) = -\sigma_{\alpha 3}\left(\xi_1, \xi_2, -\frac{h}{2}\right),\\
&\sigma^+(\xi_1, \xi_2) = \sigma_{33}\left(\xi_1, \xi_2, \frac{h}{2}\right)\\
&\text{and } \sigma^-(\xi_1, \xi_2) = -\sigma_{33}\left(\xi_1, \xi_2, -\frac{h}{2}\right).
\end{aligned} \tag{27}$$

The obtained stress field in a classical model of moderately thick shells (such as that based on a displacement approach and presented by Reddy in [19]) does not verify these conditions.

5. Generalized Fields and Equations

5.1. Generalized Displacements, Equilibrium Equations, Strains, and Stress Boundary Conditions. The application of the stress approximation in the Hellinger-Reissner functional in (12) makes the term $\int_\Omega (\mathbf{div}\,\boldsymbol{\sigma}^* \cdot \mathbf{u}^* + \mathbf{f} \cdot \mathbf{u}^*) d\Omega$ become

$$\begin{aligned}
&\int_\omega \left(\underline{\mathbf{div}}\ \underline{\underline{\mathbf{N}}}^* + \underline{\underline{\boldsymbol{\kappa}}} \cdot \underline{\mathbf{Q}}^* + \frac{h}{2}(\kappa_1 + \kappa_2)(\underline{\boldsymbol{\tau}}^+ - \underline{\boldsymbol{\tau}}^-) + \underline{\boldsymbol{\tau}}^+ + \underline{\boldsymbol{\tau}}^- \right) \cdot \underline{\mathbf{U}}^* d\omega + \int_\omega \left(\operatorname{div} \underline{\mathbf{Q}}^* + \frac{\sigma^+ - \sigma^-}{2} h(\kappa_1 + \kappa_2) \right.\\
&\left. + \sigma^+ + \sigma^- - N_{11}^*\kappa_1 - N_{22}^*\kappa_2 \right) U_3^* d\omega + \int_\omega \left(\underline{\mathbf{div}}\ \underline{\underline{\mathbf{M}}}^* - \underline{\mathbf{Q}}^* + \frac{h^2}{4}(\kappa_1 + \kappa_2)(\underline{\boldsymbol{\tau}}^+ + \underline{\boldsymbol{\tau}}^-) + \frac{h}{2}(\underline{\boldsymbol{\tau}}^+ - \underline{\boldsymbol{\tau}}^-) \right)\\
&\cdot \underline{\boldsymbol{\Phi}}^* d\omega + \int_\omega \left(h\underline{\mathbf{f}} \cdot \underline{\mathbf{U}}^* + hf_3U_3^* + \frac{h^3(\kappa_1 + \kappa_2)}{12}\underline{\mathbf{f}} \cdot \underline{\boldsymbol{\Phi}}^* \right) d\omega
\end{aligned} \tag{28}$$

where $\underline{\mathbf{f}} = f_1\mathbf{e_1} + f_2\mathbf{e_2}$,

$$U_3^* = \int_{-h/2}^{h/2} \frac{P_0}{h} u_3^* d\xi_3, \tag{29}$$

$\underline{\mathbf{U}}^*$ and $\underline{\boldsymbol{\Phi}}^*$ are 2D vectors whose components are defined on the basis of lines of curvature as follows:

$$\begin{aligned}
\underline{\mathbf{U}}^* &= \begin{pmatrix} U_1^* \\ U_2^* \end{pmatrix},\\
U_1^* &= \int_{-h/2}^{h/2} \frac{P_0}{h} u_1^* d\xi_3,\\
U_2^* &= \int_{-h/2}^{h/2} \frac{P_0}{h} u_2^* d\xi_3,\\
\underline{\boldsymbol{\Phi}}^* &= \begin{pmatrix} \phi_1^* \\ \phi_2^* \end{pmatrix},\\
\phi_1^* &= \int_{-h/2}^{h/2} \frac{12P_1}{h^2} u_1^* d\xi_3,\\
\phi_2^* &= \int_{-h/2}^{h/2} \frac{12P_1}{h^2} u_2^* d\xi_3.
\end{aligned} \tag{30}$$

Expression (28) allows identifying the following 5 generalized displacements: U_1^*, U_2^*, U_3^*, ϕ_1^*, and ϕ_2^* (the two latter can be regarded as rotations). Let us point out that in the stress approach, the approximation of the 3D displacement field $\mathbf{u}$ is not required. Nevertheless, one can state that its components take the following array form:

$$\begin{aligned}
&\mathbf{u}\\
&= \begin{pmatrix} U_1(\xi_1, \xi_2)P_0(\xi_3) + h\phi_1(\xi_1, \xi_2)P_1(\xi_3) + \delta u_1(\xi_1, \xi_2, \xi_3) \\ U_2(\xi_1, \xi_2)P_0(\xi_3) + h\phi_2(\xi_1, \xi_2)P_1(\xi_3) + \delta u_2(\xi_1, \xi_2, \xi_3) \\ U_3(\xi_1, \xi_2)P_0(\xi_3) + \delta u_3(\xi_1, \xi_2, \xi_3) \end{pmatrix}
\end{aligned} \tag{31}$$

where δu_1, δu_2, and δu_3 verify

$$\begin{aligned}
&\int_{-h/2}^{h/2} P_i \delta u_\alpha d\xi_3 = 0 \quad \text{for } i \geq 2\\
&\text{and } \int_{-h/2}^{h/2} P_j \delta u_3 d\xi_3 = 0 \quad \text{for } j \geq 1.
\end{aligned} \tag{32}$$

The stationarity of the H.R. functional (in (12)) with respect to the generalized displacements leads to the following generalized equilibrium equations:

$$\underline{\underline{\mathbf{div}}}\ \underline{\underline{\mathbf{N}}} + \underline{\underline{\boldsymbol{\kappa}}} \cdot \underline{\mathbf{Q}} + \frac{h}{2}(\kappa_1 + \kappa_2)(\underline{\boldsymbol{\tau}}^+ - \underline{\boldsymbol{\tau}}^-) + \underline{\boldsymbol{\tau}}^+ + \underline{\boldsymbol{\tau}}^- + h\underline{\mathbf{f}} = \underline{\mathbf{0}}, \tag{33}$$

$$\mathrm{div}\,\underline{\mathbf{Q}} + \frac{\sigma^+ - \sigma^-}{2} h(\kappa_1 + \kappa_2) + \sigma^+ + \sigma^- - N_{11}\kappa_1 - N_{22}\kappa_2 + hf_3 = 0, \tag{34}$$

$$\underline{\mathbf{div}}\ \underline{\underline{\mathbf{M}}} - \underline{\mathbf{Q}} + \frac{h^2}{4}(\kappa_1 + \kappa_2)(\underline{\boldsymbol{\tau}}^+ + \underline{\boldsymbol{\tau}}^-) + \frac{h}{2}(\underline{\boldsymbol{\tau}}^+ - \underline{\boldsymbol{\tau}}^-) + \frac{h^3(\kappa_1 + \kappa_2)}{12}\underline{\mathbf{f}} = \underline{\mathbf{0}}. \tag{35}$$

Let us point out that in other shell models such as that in [19], a supplementary algebraic equilibrium equation is considered:

$$M_{12}\kappa_2 - M_{21}\kappa_1 = N_{21} - N_{12}. \tag{36}$$

In SAM-H model, this equation is not considered as an equilibrium equation. Equations (21) will be considered in the constitutive equations (C.4) of SAM-H model and, with this consideration, it can be easily verified that condition (36) is automatically satisfied by making use of assumption (3).

The aforementioned stationarity for the boundary integral

$$\int_{\partial\Omega_s} (\boldsymbol{\sigma}^* \cdot \mathbf{n} - \mathbf{s}^{\mathbf{g}}) \cdot \mathbf{u}^* dS \tag{37}$$

in the H.R. functional provides the boundary conditions on the generalized forces. Let us point out that the term $\boldsymbol{\sigma}^* \cdot \mathbf{n} - \mathbf{s}^{\mathbf{g}}$ is zero on the inner and outer faces of the shell due to (27). Thus, the boundary integral reduces to an integration on the lateral boundaries (not the faces) of the structure. At these lateral boundaries, the following assumptions are adopted for the stress vector $\mathbf{s}^{\mathbf{g}}$: the first and second components of this vector (s_1^g and s_2^g) are first degree ξ_3-polynomials, while the third component (s_3^g) is uniform through the thickness of the shell. Owing to these assumptions and to assumption (3) in Section 2, the aforementioned stationarity yields the boundary conditions on the generalized forces:

$$\underline{\underline{\mathbf{N}}} \cdot \underline{\mathbf{n}}^0 = \underline{\mathbf{F}}^g, \quad \underline{\mathbf{Q}} \cdot \underline{\mathbf{n}}^0 = F_3^g, \quad \underline{\underline{\mathbf{M}}} \cdot \underline{\mathbf{n}}^0 = \underline{\mathbf{C}}^g. \tag{38}$$

Here $\underline{\mathbf{F}}^g$, F_3^g, and $\underline{\mathbf{C}}^g$ are the given membrane force vector, shear force, and bending moment vector at the shell edges, respectively. Their components are

$$F_\alpha^g = \int_{-h/2}^{h/2} \left[P_0 + h\left(\left(n_1^0\right)^2 \kappa_1 + \left(n_2^0\right)^2 \kappa_2\right) P_1\right] s_\alpha^g d\xi_3,$$

$$F_3^g = \int_{-h/2}^{h/2} \left[P_0 + h\left(\left(n_1^0\right)^2 \kappa_1 + \left(n_2^0\right)^2 \kappa_2\right) P_1\right] s_3^g d\xi_3$$

$$\text{and } C_\alpha^g = \int_{-h/2}^{h/2} \frac{h^2}{12}\left(\left(n_1^0\right)^2 \kappa_1 + \left(n_2^0\right)^2 \kappa_2\right) P_0(\xi_3)\, s_\alpha^g d\xi_3 + \int_{-h/2}^{h/2} hP_1(\xi_3)\left[1 - \frac{h}{6}\left(\left(n_1^0\right)^2 \kappa_1 + \left(n_2^0\right)^2 \kappa_2\right)\right] \cdot s_\alpha^g d\xi_3. \tag{39}$$

Once the generalized displacements are identified, by means of an integration by parts the term $-\int_\Omega (\mathbf{div}\,\boldsymbol{\sigma}^* \cdot \mathbf{u}^* + \mathbf{f} \cdot \mathbf{u}^*) d\Omega$ in the H.R. functional becomes

$$\int_\omega \left(\underline{\underline{\mathbf{N}}}^* : \underline{\underline{\boldsymbol{\varepsilon}}}^{*t} + \underline{\mathbf{Q}}^* \cdot \underline{\mathbf{d}}^* + \underline{\underline{\mathbf{M}}}^* : \underline{\underline{\boldsymbol{\chi}}}^{*t}\right) d\omega + T \tag{40}$$

where the superscript ^{t} denotes the transposition of a tensor; T is a term involving the generalized forces and displacements evaluated at the edges of the middle surface ω; $\underline{\underline{\boldsymbol{\varepsilon}}}^*$, $\underline{\underline{\boldsymbol{\chi}}}^*$, and $\underline{\mathbf{d}}^*$ are the generalized strain tensors defined as follows:

$$\underline{\underline{\boldsymbol{\varepsilon}}}^* = \underline{\underline{\mathbf{grad}}}\,\underline{\mathbf{U}}^* + U_3^* \underline{\underline{\boldsymbol{\kappa}}}, \quad \underline{\underline{\boldsymbol{\chi}}}^* = \underline{\underline{\mathbf{grad}}}\,\underline{\boldsymbol{\Phi}}^*, \quad \underline{\mathbf{d}}^* = \underline{\mathbf{grad}}\,U_3^* + \underline{\boldsymbol{\Phi}}^* - \underline{\underline{\boldsymbol{\kappa}}} \cdot \underline{\mathbf{U}}^*. \tag{41}$$

5.2. Generalized Constitutive Equations and Displacement Boundary Conditions. Let us now introduce the stress approximation in the expression of the volume elastic energy density w_e^* in (12). The integral of this energy can be written as follows:

$$\int_\Omega w_e^* d\Omega = \int_\omega \left(w_e^{s*} + w_e^{n*} + w_e^{Q*} + w_e^{c*}\right) d\omega \tag{42}$$

where w_e^{s*}, w_e^{n*}, w_e^{Q*}, and w_e^c are the surface densities of elastic energy due to in-plane stresses $\sigma_{\alpha\beta}$, elastic energy due to normal out-of-plane stresses σ_{33}, elastic energy due to out-of-plane shear stresses $\sigma_{\alpha 3}$, and elastic energy due to coupling between in-plane stresses and normal out-of-plane stresses, respectively. Let us point out that in moderately thick plate models and shell models, w_e^c is neglected; this energy accounts for the 3D Poisson's effect of normal stresses σ_{33} on in-plane strains. Owing to the definitions of compliance tensors and constants in (9), these surface densities of energy are defined by

$$w_e^{s*} = \frac{1}{2}\int_{-h/2}^{h/2} \underline{\underline{\boldsymbol{\sigma}}}^* : \underline{\underline{\underline{\underline{\mathbf{S}}}}} : \underline{\underline{\boldsymbol{\sigma}}}^* (1 + \xi_3\kappa_1)(1 + \xi_3\kappa_2)\, d\xi_3$$

$$w_e^{n*} = \frac{1}{2}\int_{-h/2}^{h/2} \sigma_{33}^* S^\sigma \sigma_{33}^* (1 + \xi_3\kappa_1)(1 + \xi_3\kappa_2)\, d\xi_3,$$

$$w_e^{Q*} = \frac{1}{2}\sum_{\alpha=1}^{2}\sum_{\beta=1}^{2}\int_{-h/2}^{h/2}\sigma_{\alpha_3}^{*}S_{\alpha\beta}^{Q}\sigma_{\beta_3}^{*}\left(1+\xi_3\kappa_1\right)\left(1+\xi_3\kappa_2\right)d\xi_3$$

and w_e^{c*}

$$= \frac{1}{2}\int_{-h/2}^{h/2}\left(\underline{\underline{\boldsymbol{\sigma}}}^{*} : \underline{\underline{\mathbf{S}}}^{\mathbf{c}}\right)\sigma_{33}^{*}\left(1+\xi_3\kappa_1\right)\left(1+\xi_3\kappa_2\right)d\xi_3. \tag{43}$$

Let us express the surface densities of energy as algebraic functions of the generalized forces, the third component of the body load (f_3), and the components of the stress vectors applied at the shell faces ($\mathbf{s}^+$ and $\mathbf{s}^-$). Let us first apply in the equations above the stress approximation detailed in (15)–(17) and its corresponding stress coefficients determined in (A.1)–(A.3) in Appendix A, B, and C. Some terms in these stress coefficients yield directly the desired algebraic combinations, and the others involve the following divergences:

(i) $\operatorname{div}\underline{\mathbf{Q}}^{*}$, $h\operatorname{div}(\underline{\underline{\boldsymbol{\kappa}}}'\cdot\underline{\mathbf{Q}}^{*})$, $h\operatorname{div}(\underline{\underline{\boldsymbol{\kappa}}}\cdot\underline{\mathbf{Q}}^{*})$,

(ii) $\underline{\mathbf{div}}(\underline{\underline{\mathbf{M}}}^{*}\cdot\underline{\underline{\boldsymbol{\kappa}}}')$, $h\operatorname{div}[\underline{\mathbf{div}}(\underline{\underline{\mathbf{M}}}^{*}\cdot\underline{\underline{\boldsymbol{\kappa}}}')]$,

(iii) $\operatorname{div}\underline{\boldsymbol{\tau}}^{+}$, $\operatorname{div}\underline{\boldsymbol{\tau}}^{-}$, $\operatorname{div}(\underline{\underline{\boldsymbol{\kappa}}}'\cdot\underline{\boldsymbol{\tau}}^{+})$, $\operatorname{div}(\underline{\underline{\boldsymbol{\kappa}}}\cdot\underline{\boldsymbol{\tau}}^{+})$, $\operatorname{div}(\underline{\underline{\boldsymbol{\kappa}}}'\cdot\underline{\boldsymbol{\tau}}^{-})$ and $\operatorname{div}(\underline{\underline{\boldsymbol{\kappa}}}\cdot\underline{\boldsymbol{\tau}}^{-})$.

These divergences can be expressed as linear algebraic functions of the generalized forces and f_3. In this manner, one obtains that w_e^{*} is a quadratic function of the algebraic values of the components of $\mathbf{f}$, $\mathbf{s}^+$, $\mathbf{s}^-$ and the generalized forces.

By making use of the stationarity of the H.R. functional with respect to the generalized forces, one obtains the generalized constitutive equations in a tensor form. It is easier to write the generalized constitutive equations in terms of the following engineering vectors of generalized forces $\mathbf{q}$ and strains $\boldsymbol{\epsilon}$:

$$\mathbf{q} = \begin{pmatrix}\widehat{\mathbf{N}}\\ \widehat{\mathbf{M}}\end{pmatrix}, \qquad \boldsymbol{\epsilon} = \begin{pmatrix}\widehat{\boldsymbol{\varepsilon}}\\ \widehat{\boldsymbol{\chi}}\end{pmatrix}, \tag{44}$$

where

$$\widehat{\mathbf{N}} = \begin{pmatrix}N_{11}\\ N_{22}\\ N_{12}\\ N_{21}\end{pmatrix}, \qquad \widehat{\mathbf{M}} = \begin{pmatrix}M_{11}\\ M_{22}\\ M_{12}\\ M_{21}\end{pmatrix},$$

$$\widehat{\boldsymbol{\varepsilon}} = \begin{pmatrix}\varepsilon_{11}\\ \varepsilon_{22}\\ \varepsilon_{12}\\ \varepsilon_{21}\end{pmatrix}, \quad \text{and } \widehat{\boldsymbol{\chi}} = \begin{pmatrix}\chi_{11}\\ \chi_{22}\\ \chi_{12}\\ \chi_{21}\end{pmatrix}. \tag{45}$$

In this manner, the constitutive equations can be grouped in two vector equations:

$$\boldsymbol{\epsilon} = \mathbf{C}\mathbf{q} + \sigma^{+}\mathbf{c}^{+} + \sigma^{-}\mathbf{c}^{-} + f_3\mathbf{c}^{\mathbf{3}}$$
$$\text{and } \underline{\mathbf{d}} = \mathbf{D}\underline{\mathbf{Q}} + \mathbf{D}^{+}\underline{\boldsymbol{\tau}}^{+} + \mathbf{D}^{-}\underline{\boldsymbol{\tau}}^{-}, \tag{46}$$

where

(i) $\mathbf{C}$ is an 8×8 compliance matrix,

(ii) $\mathbf{c}^{+}$, $\mathbf{c}^{-}$, and $\mathbf{c}^{\mathbf{3}}$ are 8-component compliance vector,

(iii) $\mathbf{D}$, $\mathbf{D}^{+}$, and $\mathbf{D}^{-}$ are 2×2 compliance matrices.

The components of these matrices and vectors are provided in Appendix B.

Appendix C proves that there is an alternative form of the constitutive equations which expresses the generalized forces as linear combinations of the generalized strains and the applied loads.

The constitutive equations can be grouped in the following two vector equations:

$$\mathbf{q} = \mathbf{K}\boldsymbol{\epsilon} + \sigma^{+}\mathbf{k}^{+} + \sigma^{-}\mathbf{k}^{-} + f_3\mathbf{k}^{\mathbf{3}},$$
$$\underline{\mathbf{Q}} = \mathbf{L}\underline{\mathbf{d}} + \mathbf{L}^{+}\underline{\boldsymbol{\tau}}^{+} + \mathbf{L}^{-}\underline{\boldsymbol{\tau}}^{-}. \tag{47}$$

The expressions of the above matrices ($\mathbf{K}$, $\mathbf{L}$, $\mathbf{L}^{+}$, and $\mathbf{L}^{-}$) and vectors ($\mathbf{k}^{+}$, $\mathbf{k}^{-}$, and $\mathbf{k}^{\mathbf{3}}$) are shown in Appendix C. The resulting N_{21} and M_{21} generalized forces obtained by means of (47) verify (21) and the supplementary algebraic "equilibrium" (36) included in Sanders model [14].

The stationarity of the H.R. functional (in (11)) with respect to the generalized forces also provides in the $-\int_{\partial\Omega_{\mathbf{u}}}(\boldsymbol{\sigma}^{*}\cdot\mathbf{n})\cdot(\mathbf{u}^{*}-\mathbf{u}^{\mathbf{g}})dS$ term the generalized displacement boundary conditions on the edge of the shell:

$$\underline{\mathbf{U}} = \int_{-h/2}^{h/2}\frac{P_0}{h}\left(u_1^{g}\mathbf{e_1} + u_2^{g}\mathbf{e_2}\right)d\xi_3,$$
$$U_3 = \int_{-h/2}^{h/2}\frac{P_0}{h}u_3^{g}d\xi_3, \tag{48}$$
$$\underline{\boldsymbol{\Phi}} = \int_{-h/2}^{h/2}\frac{12P_1}{h^2}\left(u_1^{g}\mathbf{e_1} + u_2^{g}\mathbf{e_2}\right)d\xi_3.$$

6. Results and Discussion

6.1. Main Differences with a Classical Model of Shells. In [19], Reddy builds a model of homogeneous general shells (from thin to moderately thick) which generalizes Sanders shell theory [14]. The generalization consists of including von Kármán nonlinear strains. In order to compare the linear SAM-H model to Reddy's model, the nonlinear terms are not considered herein. Hereafter, the linear version of Reddy's model will be referred to as the classical shell model (CS model). The CS model is based on an approximation of the 3D displacement field components in the curvilinear coordinate system:

$$\begin{aligned} u_\alpha(\xi_1,\xi_2,\xi_3) &= U_\alpha^c(\xi_1,\xi_2) + h\phi_\alpha^c P_1(\xi_3) \\ u_3(\xi_1,\xi_2,\xi_3) &= U_3^c(\xi_1,\xi_2) \end{aligned} \tag{49}$$

which involves 5 generalized displacements (U_1^c, U_2^c, U_3^c, ϕ_1^c, ϕ_2^c). The first 3 generalized displacements are the 3D displacements at the middle surface. The 5 generalized displacements can be expressed as thickness integrals of the 3D displacements in a similar manner to that in (29) and (30). In this sense, the generalized displacements of the SAM-H model are equivalent to those of the classical shell model (CS model). SAM-H model does not propose an approximation of the 3D displacements but it has the same number of generalized displacements as the CS model. From SAM-H generalized displacements, one may obtain some characteristics of the 3D displacement field. By applying the 3D gradient to the 3D displacement field in (49), one obtains the 3D strains of the CS model. Let us point out that the 3D linear normal strain component ε_{33} is zero. These 3D strains can be expressed as linear algebraic combinations of the generalized strains of the CS model. The generalized strains are related to the 2D gradients of the generalized displacements of the CS model in a similar manner as in the SAM-H model (see (41)):

$$\begin{aligned} \underline{\underline{\boldsymbol{\varepsilon}}}^c &= \underline{\underline{\mathbf{grad}}}\ \underline{\mathbf{U^c}} + U_3^c\underline{\underline{\boldsymbol{\kappa}}}, \\ \underline{\underline{\boldsymbol{\chi}}}^c &= \underline{\underline{\mathbf{grad}}}\ \underline{\boldsymbol{\Phi}^c}, \\ \underline{\mathbf{d}}^c &= \underline{\mathbf{grad}}\ U_3^c + \underline{\boldsymbol{\Phi}}^c - \underline{\underline{\boldsymbol{\kappa}}}\cdot\underline{\mathbf{U^c}}. \end{aligned} \tag{50}$$

Let us point out that the SAM-H model does not propose any approximation of the 3D strain tensor. By applying Hamilton's variational principle to the shell, Reddy obtains the generalized equilibrium equations of the CS model [19].

$$\begin{aligned} \underline{\mathbf{div}}\ \underline{\underline{\mathbf{N^c}}} + \underline{\underline{\boldsymbol{\kappa}}}\cdot\underline{\mathbf{Q^c}} + \underline{\mathbf{f^{eq}}} &= \mathbf{0} \\ \operatorname{div}\underline{\mathbf{Q^c}} - N_{11}^c\kappa_1 - N_{22}^c\kappa_2 + f_3^{eq} &= 0 \\ \underline{\mathbf{div}}\ \underline{\underline{\mathbf{M^c}}} - \underline{\mathbf{Q^c}} &= \mathbf{0} \end{aligned} \tag{51}$$

where $\underline{\underline{\mathbf{N^c}}}$, $\underline{\mathbf{Q^c}}$, and $\underline{\underline{\mathbf{M^c}}}$ are the generalized forces of the CS model and have a definition similar to those of the SAM-H model in (18) to (20); $\underline{\mathbf{f^{eq}}}$ and f_3^{eq} are the equivalent middle surface in-plane and out-of-plane loads, respectively. The additional equilibrium equation (36) in Sanders model [14] is also considered.

The equivalent middle surface loads can model the effect of the body loads and the loads applied at the faces of the shell. Let us point out that in SAM-H model, the body loads and the applied stresses on the faces appear explicitly in its equations. Besides, in SAM-H model, in some terms of the equilibrium equations, these loads and stresses are multiplied by the principal curvatures, and the loads applied on the inner and outer faces of the shell are distinguished.

In the CS model, after obtaining the approximate 3D strains, the 3D constitutive equations for a homogeneous shell yield the stress field approximation. The CS model neglects out-of-plane normal stresses σ_{33}. An integration through the thickness yields the generalized constitutive equations:

$$\begin{aligned} &\begin{pmatrix} \widehat{\mathbf{N^c}} \\ \widehat{\mathbf{M^c}} \end{pmatrix} = \begin{pmatrix} \mathbf{A^c} & \mathbf{B^c} \\ \mathbf{B^c} & \mathbf{D^c} \end{pmatrix} \cdot \begin{pmatrix} \widehat{\boldsymbol{\varepsilon}^c} \\ \widehat{\boldsymbol{\chi}^c} \end{pmatrix} \\ &\text{and } \underline{\mathbf{Q^c}} = \underline{\underline{\mathbf{K^c}}}\cdot\underline{\mathbf{d^c}}, \end{aligned} \tag{52}$$

where $\widehat{\mathbf{N^c}}$, $\widehat{\mathbf{M^c}}$, $\widehat{\boldsymbol{\varepsilon}^c}$, and $\widehat{\boldsymbol{\chi}^c}$ have definitions analogue to those in (45); $\mathbf{A^c}$, $\mathbf{B^c}$, $\mathbf{D^c}$, and $\underline{\underline{\mathbf{K^c}}}$ are stiffness matrices. Let us point out that in the CS model an "ABBD" stiffness matrix appears while an "ABCD" stiffness matrix is expected in the SAM-H model (see the expression of the generalized compliance matrices in (B.1)). Another difference is the fact that in the CS model, the constitutive equations do not involve the body loads and the loads applied at the faces of the shell; in SAM-H model, these loads appear explicitly in the constitutive equations. The Poisson's effects of the out-of-plane normal stresses on in-plane strains are considered in the SAM-H model but not in the CS model.

6.2. Analytical Results. Let us now compare the analytical solutions of the CS and SAM-H models in the case of a hollow sphere subjected to an internal pressure p. The thickness of the sphere is h; the radius of the middle surface is R. The material is isotropic, and its Young's modulus and Poisson's ratio are, respectively, E and ν. Vector $\mathbf{e_3}$ points from inside to outside the sphere. The analytical resolution of the 3D problem with spherical symmetry leads to the following radial displacement (u_3) and normal stress σ_{33}:

$$u_3^{3D}\left(\bar{\xi}_3\right) = \frac{pR}{E}\left[\frac{(1-\eta/2)^3\left(2(1-2\nu)\left(1+\eta\bar{\xi}_3\right)^3 + (1+\nu)(1+\eta/2)^3\right)}{2\left((1+\eta/2)^3 - (1-\eta/2)^3\right)\left(1+\eta\bar{\xi}_3\right)^2}\right],$$

$$\text{and } \sigma_{33}^{3D}\left(\overline{\xi}_3\right) = p\frac{\left(1-\eta/2\right)^3}{\left(1+\eta/2\right)^3-\left(1-\eta/2\right)^3}\left(1-\left(\frac{1+\eta/2}{1+\eta\overline{\xi}_3}\right)^3\right), \tag{53}$$

where $\eta = h/R$ is the thickness to radius ratio and $\overline{\xi}_3 = \xi_3/h$ is the normalized position through the thickness. The analytical resolution of the equations of the CS model yields the generalized displacement and the normal stress:

$$U_3^{CS} = \frac{pR}{E}\left[\frac{1-\nu}{2\eta}\right] \quad \text{and } \sigma_{33}^{CS} = 0. \tag{54}$$

The generalized displacement and normal stress of the SAM-H model are

$$U_3^{SAM} = U_3^{CS} - \frac{pR}{E}\left(\frac{1-2\nu}{2}+\frac{3}{140}\eta+\frac{13\nu}{30}\eta+\frac{\nu}{10}\eta^2\right), \quad \text{and } \sigma_{33}^{SAM}\left(\overline{\xi}_3\right) = p\left(-\frac{1-\eta}{2}+\overline{\xi}_3-2\overline{\xi}_3^2\eta+\frac{\eta^2}{8}-\frac{\eta^2\overline{\xi}_3^2}{2}\right). \tag{55}$$

Let us first compare the displacement solutions of the CS and SAM-H models with the mean 3D displacement

$$U_3^{3D} = \int_{-h/2}^{h/2}\frac{P_0}{h}u_3^{3D}\left(\frac{\xi_3}{h}\right)d\xi_3 = \frac{pR}{E}\left[\frac{2\left(1-\eta/2\right)^3\left(1-2\nu\right)+\left(1-\eta/2\right)^2\left(1+\eta/2\right)^2\left(1+\nu\right)}{2\left(\left(1+\eta/2\right)^3-\left(1-\eta/2\right)^3\right)}\right]. \tag{56}$$

Let us define the relative errors

$$\delta U_3^{SAM} = \frac{U_3^{SAM}-U_3^{3D}}{U_3^{3D}} \quad \text{and } \delta U_3^{CS} = \frac{U_3^{CS}-U_3^{3D}}{U_3^{3D}} \tag{57}$$

in the evaluation of the mean displacement for the CS and SAM-H models. These errors only depend on η and ν. In Figures 2(a) and 2(b), the relative errors δU_3^{SAM} and δU_3^{CS} are plotted against the thickness to radius ratio η for five values of the Poisson's ratio (-0.4, -0.2, 0, 0.2, and 0.4), respectively. The maximum value of the thickness to radius ratio considered in this example is 0.5; for moderately thick shells, this ratio is less than 0.3 (this limit will be justified below). The absolute value of the relative error δU_3^{SAM} of the SAM-H model increases as η and ν increase but is less than 4% for moderately thick shells and less than 14% for thicker shells. The relative error δU_3^{CS} of the CS model increase as η increases and ν decreases; it may be more than 50% for moderately thick shells and more than 100% for thicker shells. The SAM-H model provides a far better approximation than the CS model for the mean normal displacement. Let us point out that SAM-H accuracy in the prediction of U_3 is mainly due to the consideration of the elastic energy w_e^c (see (43)) corresponding to the coupling between in-plane stresses and normal out-of-plane stresses. In Figure 3, the relative error δU_3^{SAM} in the calculation of U_3 without taking into account w_e^c is plotted against η for five values of the Poisson's ratio (-0.4, -0.2, 0, 0.2, and 0.4). Neglecting w_e^c can make this error greater than 20% for the thickest moderately thick shell ($\eta = 0.3$); this value is 5 times greater than that considering w_e^c. This confirms the utility of taking into account w_e^c (the Poisson's effect of the out-of-plane normal stresses on in-plane strains). In what follows, this energy is taken into account in the SAM-H model results.

Let us now analyze the normal stresses σ_{33}. In the CS model, these stresses are zero. The SAM-H model predicts nonzero σ_{33} stresses and in order to compare the SAM-H model results to those of the 3D case, the normalized stresses σ_{33}/p are analyzed. In Figure 4, the normalized stresses calculated by the SAM-H model and the 3D model are plotted against the dimensionless position $\overline{\xi}_3$ for three values of the thickness to radius ratio: $\eta = 0.1$, 0.3, and 0.5. One can observe that the accuracy of the SAM-H results decreases as η increases. In spite of this, the SAM-H results are very accurate even for the thickest case ($\eta = 0.5$) and the boundary conditions at the inner ($\overline{\xi}_3 = -0.5$) and outer ($\overline{\xi}_3 = 0.5$) faces of the shell are verified.

6.3. Numerical Results. In this subsection, SAM-H model equations are solved by means of the finite element method implemented in COMSOL Multiphysics software (5.3 version). To test the accuracy of SAM-H model, its results are compared to those obtained with

(i) solid finite elements (SFE) available in COMSOL Multiphysics;

(ii) the classical shell model (CS model); its equations are implemented in COMSOL Multiphysics in a similar manner to how SAM-H equations were treated;

(iii) MITC6 shell finite elements [33] (triangular elements) available in COMSOL Multiphysics.

Let us consider a 2m tall hollow cylinder. The radius of the midsurface and the wall thickness are 1m and 0.3m, respectively. A 1MPa pressure is applied on a 0.25m tall circumferential section at the outer face of the cylinder. The resolution of the problem using solid finite elements (SFE) can be simplified due to symmetries as shown in Figure 5(a). The shell-type computations (SAM-H, CS, and MITC6) use

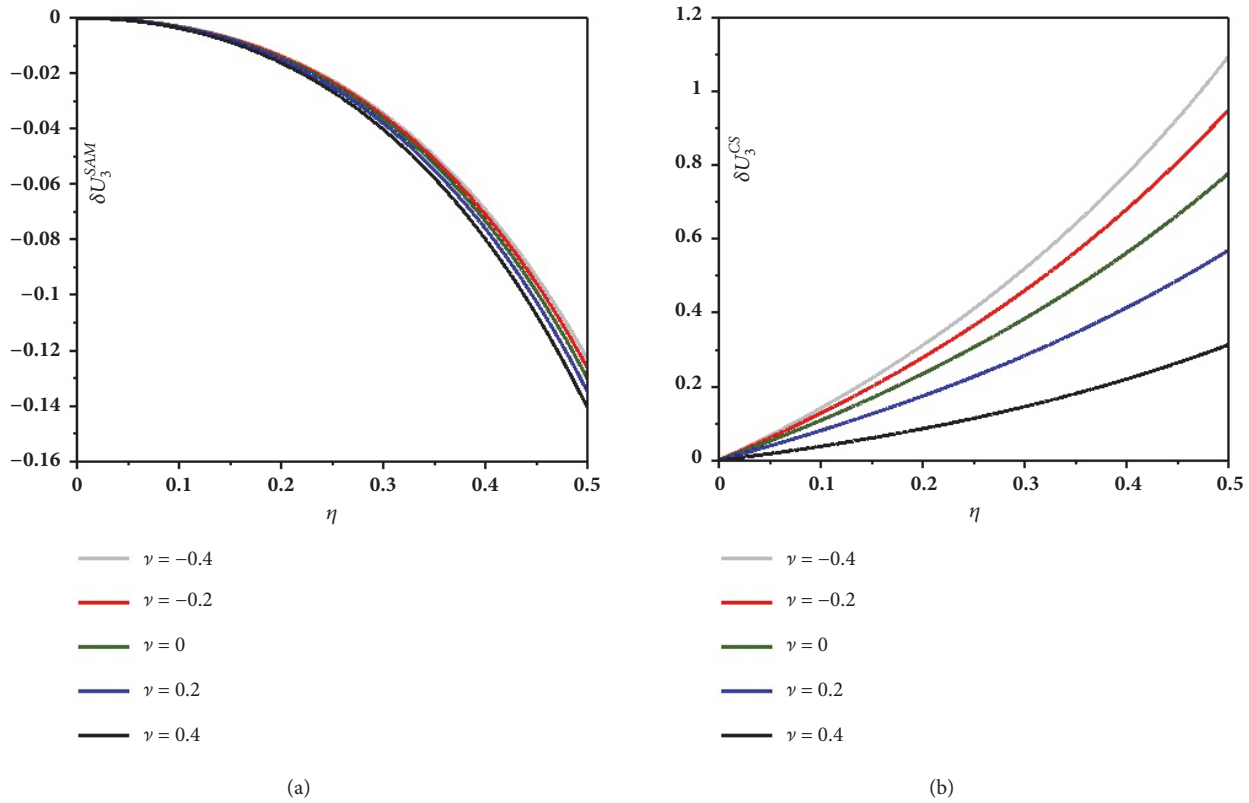

Figure 2: Relative displacement errors vs thickness to radius ratio for the SAM-H (a) and CS (b) models.

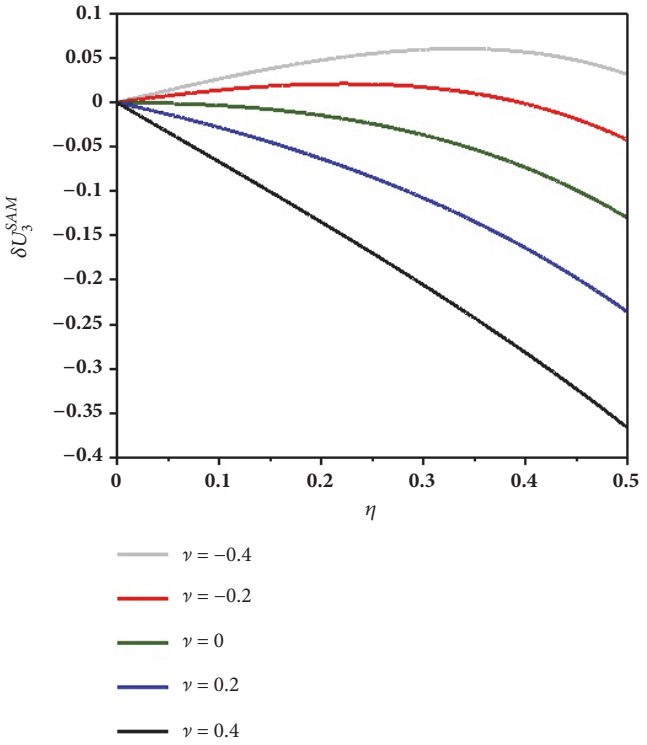

Figure 3: Relative displacement error vs thickness to radius ratio for the SAM-H without taking into account w_e^c.

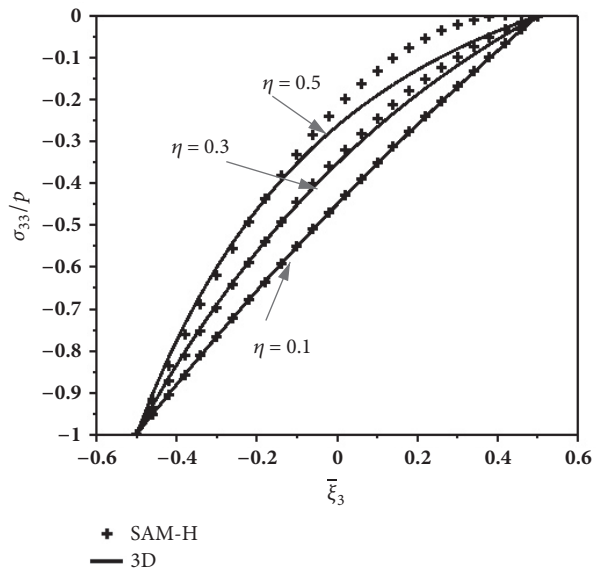

Figure 4: Normalized 3D and SAM-H normal stresses σ_{33}/p vs dimensionless position $\overline{\xi}_3$.

the mesh shown in Figure 5(b). The material is isotropic and its Young's modulus and Poisson's ratio are 200GPa and 0.3.

The resolution of the generalized equations of SAM-H and CS models allows building the approximate 3D stress field and plotting the stress components on the cross section of the cylinder drawn in Figure 5. COMSOL Multiphysics offers the possibility of obtaining from the MITC6 results the 3D stress field in a given position through the thickness of the solid. In Figure 6, the normal stresses σ_{rr} calculated by solid finite elements (SFE), the shell models (SAM-H and CS), and MITC6 shell elements are plotted on the cross section. The σ_{rr} stresses calculated by the CS model and MITC6 method are neglected whereas that calculated by SAM-H varies across the thickness in a similar manner to the SFE stress. The pressure application on a delimited portion of the outer face provokes the existence of a σ_{rz} shear stress. In Figure 7, the color maps of the calculated σ_{rz} stresses by SFE, SAM-H, CS, and MITC6 methods are plotted on the cross section of the cylinder. The CS model predicts a constant through thickness shear stress whereas SAM-H model yields a variable shear stress that verifies the boundary conditions at the inner and outer faces, in a similar manner to the MITC6 method. The values of the σ_{rz} stress calculated with SAM-H model seem more to the SFE results than those calculated with the CS model. In Figure 8, the von Mises stresses obtained by SFE, SAM-H, CS, and MITC6 are plotted on the cross section of the cylinder. Once again, one can note that SAM-H results are more accurate than those of the CS model and MITC6 method. The maximum von Mises stress at the inner face of the cylinder calculated by SFE, SAM-H, CS, and MITC6 methods is 2.15MPa, 2.10MPa, 1.91 MPa, and 1.63MPa, respectively. In Figure 8, it can be seen that the location of the maximum value of the von Mises stress is at the inner face of the shell for SFE and SAM-H models while that for CS model is at the outer face of the shell. SAM-H provides a better stress approximation than the CS and MITC6 methods for this mechanical problem.

7. Conclusions

To conclude, a new model of linear homogeneous shells (from thin to moderately thick) called SAM-H was developed in this paper. Hellinger-Reissner's functional was applied to build the model equations and fields. The model is based on a polynomial approximation of the stress field across the shell thickness. The stress field verifies the 3D equilibrium equation, and the coefficients of the stress polynomials are the generalized forces (membrane and shear forces) and bending moments of the model. The 3D stress boundary conditions at the faces of the shell are also verified. Hellinger-Reissner's functional allowed identifying the generalized displacements (3 displacements and 2 rotations) and strains. The stationarity of this functional with respect to the generalized displacements yielded 5 generalized equilibrium equations and the generalized boundary conditions on the forces at the edges of the shell. The stationarity with respect to the generalized forces provided the generalized constitutive equations and displacement boundary conditions at the shell's edges. As compared to the classical linear model (CS model) of general moderately thick shells adapted from Reddy's model in [19], SAM-H model involves the same number of generalized displacements, strains, and forces. The stress approximation of the CS model does not verify the 3D equilibrium equation and the 3D stress boundary conditions at the faces of the shell. SAM-H model involves, explicitly in its equilibrium and constitutive equations, the body loads and the applied stress vector at the shell faces, while the CS model involves only an equivalent middle surface load in the equilibrium equations. The constitutive equations of the SAM-H model are more accurate since they involve Poisson's effects of out-of-plane loads on in-plane strains. To prove the accuracy of the SAM-H model, the case of a pressurized hollow sphere was considered and the analytical results of the SAM-H and CS models for displacements and σ_{33} stress were compared to a 3D solid model solution. The SAM-H proved to be very accurate for moderately thick shells having a thickness to radius ratio less than 0.3. Its results are by far more accurate than the CS model. SAM-H model equations were also implemented in a finite element commercial software, and the case of the constriction of a cylinder was analyzed. The numerical results were compared to those of solid finite elements (SFE), the classical shell model (CS model), and MITC6 shell finite elements. SAM-H proved to be very accurate, it gives a better approximation of SFE results than the other shell models.

From a resolution point of view, the SAM-H model proposed in this paper is not more complex than a CS model (both have the same number of generalized displacements) but is more complete since it is able to calculate the normal out-of-plane stresses which should not be neglected in the failure prediction of shells. The higher polynomial degree of out-of plane stresses does not complicate the resolution of the SAM-H model equations; the calculation of these stresses is performed in a postprocessing stage. Another

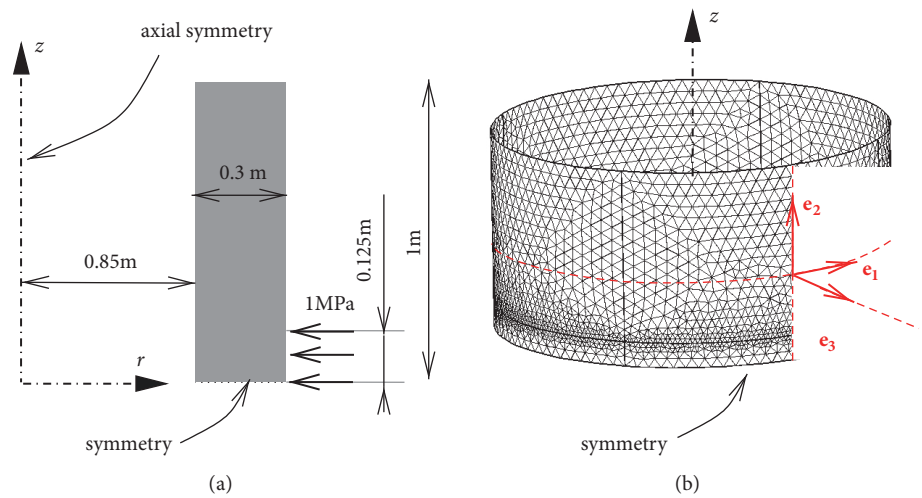

Figure 5: Constriction of a thick hollow cylinder: modelling using solid finite elements (a) and mesh for shell models (b).

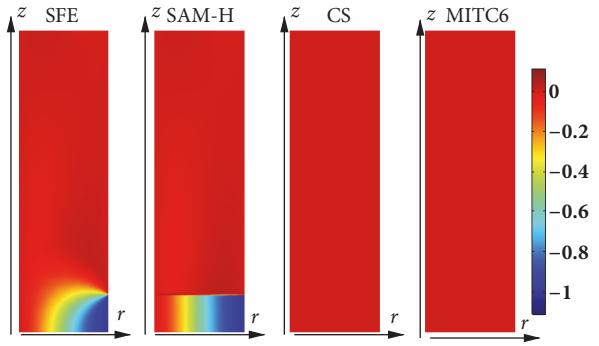

Figure 6: Normal stress σ_{rr} (in MPa) in the cross section of a constricted cylinder (SFE, SAM-H, CS, and MITC6 results).

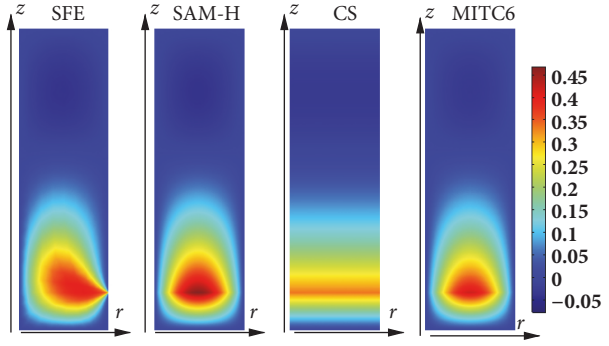

Figure 7: Shear stress σ_{rz} (in MPa) in the cross section of a constricted cylinder (SFE, SAM-H, CS, and MITC6 results).

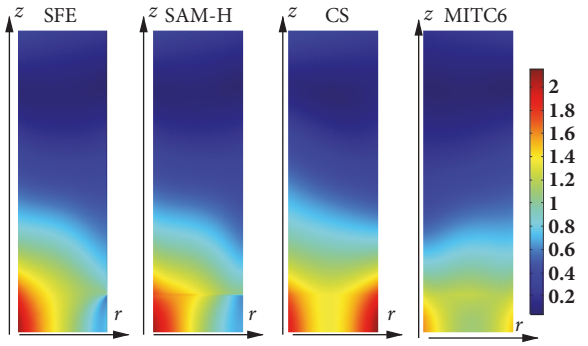

Figure 8: Von Mises stress (in MPa) in the cross section of a constricted cylinder (SFE, SAM-H, CS, and MITC6 results).

important advantage of the SAM-H model is that, while being applied to plates, it is equivalent to the extended Reissner's plate model in [13] (adapted to a homogeneous plate) that includes the above-mentioned Poisson's effects. For these reasons, the SAM-H model can be applied by engineers and implemented in commercial finite element software to obtain more accurate predictions of the structural behavior and strength of linear homogeneous shells having a moderate thickness ($\eta \leq 0.3$).

In subsequent papers, the static model developed herein will be extended so as to include dynamic effects and calculate vibration modes and eigenfrequencies of shells. Also, the same stress approach will be applied to develop new models of laminated composite shells. The consideration of geometric nonlinearities is an important topic that will also be treated in a future work.

Appendix

A. Coefficients of the Polynomial Approximation of Stresses

In this subsection, the stress coefficients in the polynomial approximations in (15)–(17) are detailed. The following expressions are obtained:

(i) for $\sigma^n_{\alpha\beta}$ $(0 \leq n \leq 1)$:

$$\sigma^0_{\alpha\beta} = \frac{1}{h}\left[\left(\underline{\underline{\mathbf{N}}} - \underline{\underline{\underline{\mathbf{M}}}} \cdot \underline{\underline{\boldsymbol{\kappa}}}'\right) \cdot \mathbf{e}_{\boldsymbol{\beta}}\right] \cdot \mathbf{e}_{\boldsymbol{\alpha}}$$
$$\text{and } \sigma^1_{\alpha\beta} = \left[\left(\frac{12}{h^2}\underline{\underline{\underline{\mathbf{M}}}} - \underline{\underline{\mathbf{N}}} \cdot \underline{\underline{\boldsymbol{\kappa}}}'\right) \cdot \mathbf{e}_{\boldsymbol{\beta}}\right] \cdot \mathbf{e}_{\boldsymbol{\alpha}}; \tag{A.1}$$

(ii) for $\sigma^n_{\alpha 3}$ $(0 \le n \le 3)$:

$$\sigma^0_{\alpha 3} = \left[\frac{1}{h}\underline{\underline{\mathbf{Q}}} - \frac{h}{12}\underline{\underline{\boldsymbol{\kappa}}}' \cdot \left(\underline{\boldsymbol{\tau}}^+ + \underline{\boldsymbol{\tau}}^-\right)\right] \cdot \mathbf{e}_{\boldsymbol{\alpha}},$$

$$\sigma^1_{\alpha 3} = \left(\underline{\boldsymbol{\tau}}^+ + \underline{\boldsymbol{\tau}}^-\right) \cdot \mathbf{e}_{\boldsymbol{\alpha}} + \frac{1}{5}\sigma^3_{\alpha 3},$$

$$\sigma^2_{\alpha 3} = \left[\frac{1}{h}\underline{\underline{\mathbf{Q}}} - \frac{1}{2}\left(\underline{\boldsymbol{\tau}}^+ - \underline{\boldsymbol{\tau}}^-\right) - \frac{h}{12}\underline{\underline{\boldsymbol{\kappa}}}' \cdot \left(\underline{\boldsymbol{\tau}}^+ + \underline{\boldsymbol{\tau}}^-\right)\right] \cdot \mathbf{e}_{\boldsymbol{\alpha}} \quad \text{(A.2)}$$

$$\text{and } \sigma^3_{\alpha 3} = \left[2\underline{\mathbf{div}}\left(\underline{\underline{\mathbf{M}}} \cdot \underline{\underline{\boldsymbol{\kappa}}}'\right) - \left(4\underline{\underline{\boldsymbol{\kappa}}} + 3\underline{\underline{\boldsymbol{\kappa}}}'\right) \cdot \left(\underline{\mathbf{Q}} - \frac{h}{2}\left(\underline{\boldsymbol{\tau}}^+ - \underline{\boldsymbol{\tau}}^-\right)\right)\right] \cdot \mathbf{e}_{\boldsymbol{\alpha}};$$

(iii) for σ^n_{33} $(0 \le n \le 4)$:

$$\sigma^0_{33} = \frac{\sigma^+ - \sigma^-}{2} + \sigma^2_{33} + \frac{1}{15}\sigma^4_{33},$$

$$\sigma^1_{33} = \sigma^+ + \sigma^- + \frac{1}{5}\sigma^3_{33},$$

$$\begin{aligned}\sigma^2_{33} &= \frac{h}{30}\mathrm{div}\left[\underline{\mathbf{div}}\left(\underline{\underline{\mathbf{M}}} \cdot \underline{\underline{\boldsymbol{\kappa}}}'\right) - 2\underline{\underline{\boldsymbol{\kappa}}} \cdot \underline{\mathbf{Q}}\right] - \frac{1}{h}\underline{\underline{\mathbf{M}}} : \underline{\underline{\boldsymbol{\kappa}}} \\ &\quad + \frac{h}{12}\mathrm{div}\left[\underline{\boldsymbol{\tau}}^+ + \underline{\boldsymbol{\tau}}^- + \frac{h}{10}\left(4\underline{\underline{\boldsymbol{\kappa}}} + 5\underline{\underline{\boldsymbol{\kappa}}}'\right) \cdot \left(\underline{\boldsymbol{\tau}}^+ - \underline{\boldsymbol{\tau}}^-\right)\right] \\ &\quad + \frac{h}{12}\left[\left(\kappa_1 + \kappa_2\right)\left(2\sigma^1_{33} - \frac{3}{5}\sigma^3_{33} + hf_3\right) - \frac{4}{5h}\sigma^4_{33}\right],\end{aligned} \quad \text{(A.3)}$$

$$\sigma^3_{33} = -\mathrm{div}\,\underline{\mathbf{Q}} + \frac{h}{4}\mathrm{div}\left[2\left(\underline{\boldsymbol{\tau}}^+ - \underline{\boldsymbol{\tau}}^-\right) - h\underline{\underline{\boldsymbol{\kappa}}} \cdot \left(\underline{\boldsymbol{\tau}}^+ + \underline{\boldsymbol{\tau}}^-\right)\right]$$

$$\text{and } \sigma^4_{33} = -\frac{3h}{14}\mathrm{div}\left[\underline{\mathbf{div}}\left(\underline{\underline{\mathbf{M}}} \cdot \underline{\underline{\boldsymbol{\kappa}}}'\right)\right] + \frac{3h}{7}\mathrm{div}\left[\left(2\underline{\underline{\boldsymbol{\kappa}}} + \underline{\underline{\boldsymbol{\kappa}}}'\right) \cdot \underline{\mathbf{Q}}\right] - \frac{3h^2}{14}\mathrm{div}\left[\left(2\underline{\underline{\boldsymbol{\kappa}}} + \underline{\underline{\boldsymbol{\kappa}}}'\right) \cdot \left(\underline{\boldsymbol{\tau}}^+ - \underline{\boldsymbol{\tau}}^-\right)\right].$$

B. Generalized Compliances

In this section, the components of the compliance matrices and vectors appearing in (46) are determined. Matrix $\mathbf{C}$ is defined by

$$\mathbf{C} = \begin{pmatrix} \mathbf{C^A} & \mathbf{C^{B1}} + \mathbf{C^{B2}} \\ \mathbf{C^{C1}} + \mathbf{C^{C2}} & \dfrac{12}{h^2}\mathbf{C^A} \end{pmatrix} \quad \text{(B.1)}$$

where

$$\mathbf{C^A} = \frac{1}{h}\begin{pmatrix} S_{1111} & S_{1122} & S_{1112} & S_{1121} \\ S_{2211} & S_{2222} & S_{2212} & S_{2221} \\ S_{1211} & S_{1222} & S_{1212} & S_{1221} \\ S_{2111} & S_{2122} & S_{2112} & S_{2121} \end{pmatrix},$$

$$\mathbf{C^{B1}} = \mathbf{C^{C1}} = \frac{\kappa_1 - \kappa_2}{h}\begin{pmatrix} S_{1111} & 0 & 0 & S_{1121} \\ 0 & -S_{2222} & -S_{2212} & 0 \\ 0 & -S_{1222} & -S_{1212} & 0 \\ S_{2111} & 0 & 0 & S_{2121} \end{pmatrix},$$

$$\mathbf{C^{B2}} = -\frac{1}{10h} \cdot \begin{pmatrix} 6S^C_{11}\kappa_1 & S^C_{22}\kappa_1 + 5S^C_{11}\kappa_2 & S^C_{12}\kappa_1 & S^C_{21}\kappa_1 \\ S^C_{11}\kappa_2 + 5S^C_{22}\kappa_1 & 6S^C_{22}\kappa_2 & S^C_{12}\kappa_2 & S^C_{21}\kappa_2 \\ 5S^C_{12}\kappa_1 & 5S^C_{12}\kappa_2 & 0 & 0 \\ 5S^C_{21}\kappa_1 & 5S^C_{21}\kappa_2 & 0 & 0 \end{pmatrix},$$

$$\mathbf{C^{C2}} = -\frac{1}{10h} \cdot \begin{pmatrix} 6S^C_{11}\kappa_1 & 5S^C_{22}\kappa_1 + S^C_{11}\kappa_2 & 5S^C_{12}\kappa_1 & 5S^C_{21}\kappa_1 \\ 5S^C_{11}\kappa_2 + S^C_{22}\kappa_1 & 6S^C_{22}\kappa_2 & 5S^C_{12}\kappa_2 & 5S^C_{21}\kappa_2 \\ S^C_{12}\kappa_1 & S^C_{12}\kappa_2 & 0 & 0 \\ S^C_{21}\kappa_1 & S^C_{21}\kappa_2 & 0 & 0 \end{pmatrix}. \quad \text{(B.2)}$$

Vectors $\mathbf{c}^+$ and $\mathbf{c}^-$ are defined by

$$\mathbf{c}^+ = -\frac{S^\sigma}{140}\begin{pmatrix} 3h\mathbf{c^a} \\ 70\mathbf{c^a} \end{pmatrix} + \frac{1}{60}\begin{pmatrix} \mathbf{C^S}\left(15\mathbf{c^b} + 8h\mathbf{c^c} + 5h\mathbf{c^d}\right) \\ \dfrac{1}{h}\mathbf{C^S}\left(36\mathbf{c^b} + 18h\mathbf{c^c} + 3h\mathbf{c^d}\right) \end{pmatrix} \quad \text{(B.3)}$$

and

$$\mathbf{c}^- = \frac{S^\sigma}{140}\begin{pmatrix} -3h\mathbf{c^a} \\ 70\mathbf{c^a} \end{pmatrix} + \frac{1}{60}\begin{pmatrix} \mathbf{C^S}\left(-15\mathbf{c^b} + 8h\mathbf{c^c} + 5h\mathbf{c^d}\right) \\ \dfrac{1}{h}\mathbf{C^S}\left(36\mathbf{c^b} - 18h\mathbf{c^c} - 3h\mathbf{c^d}\right) \end{pmatrix}, \quad \text{(B.4)}$$

where

$$\mathbf{c^a}\begin{pmatrix} \kappa_1 \\ \kappa_2 \\ 0 \\ 0 \end{pmatrix},$$

$$\mathbf{C^S} = \begin{pmatrix} S^C_{11} & 0 & 0 & 0 \\ 0 & S^C_{22} & 0 & 0 \\ 0 & 0 & S^C_{12} & 0 \\ 0 & 0 & 0 & S^C_{21} \end{pmatrix}, \quad \text{(B.5)}$$

$$\mathbf{c^b} = \begin{pmatrix} 1 \\ 1 \\ 1 \\ 1 \end{pmatrix},$$

$$\mathbf{c^c} = \begin{pmatrix} \kappa_1 \\ \kappa_2 \\ \kappa_2 \\ \kappa_1 \end{pmatrix}, \quad \text{and } \mathbf{c^d} = \begin{pmatrix} \kappa_2 \\ \kappa_1 \\ \kappa_1 \\ \kappa_2 \end{pmatrix}. \tag{B.6}$$

The compliance vector $\mathbf{c^3}$ is

$$\mathbf{c^3} = -\frac{h^2 S^\sigma}{210} \begin{pmatrix} \mathbf{c^a} \\ 0 \cdot \mathbf{c^a} \end{pmatrix} + \frac{1}{120} \begin{pmatrix} h^2 \mathbf{C^S} \left(6\mathbf{c^c} + 5\mathbf{c^d}\right) \\ 12\mathbf{C^S c^b} \end{pmatrix}. \tag{B.7}$$

The components of the shearing compliance matrices $\mathbf{D}$, $\mathbf{D}^+$, and $\mathbf{D}^-$ are given by

$$\mathbf{D} = \frac{6}{5h} \begin{pmatrix} S_{11}^{\mathrm{Q}} & S_{12}^{\mathrm{Q}} \\ S_{21}^{\mathrm{Q}} & S_{22}^{\mathrm{Q}} \end{pmatrix}, \tag{B.8}$$

$$\mathbf{D}^+ = -\frac{1}{60} \cdot \begin{pmatrix} S_{11}^{\mathrm{Q}} (6 + 5h\kappa_2) & S_{12}^{\mathrm{Q}} (6 + 6h\kappa_1 - h\kappa_2) \\ S_{21}^{\mathrm{Q}} (6 - h\kappa_1 + 6h\kappa_2) & S_{22}^{\mathrm{Q}} (6 + 5h\kappa_1) \end{pmatrix} \tag{B.9}$$

and

$$\mathbf{D}^- = \frac{1}{60} \cdot \begin{pmatrix} S_{11}^{\mathrm{Q}} (6 - 5h\kappa_2) & S_{12}^{\mathrm{Q}} (6 - 6h\kappa_1 + h\kappa_2) \\ S_{21}^{\mathrm{Q}} (6 + h\kappa_1 - 6h\kappa_2) & S_{22}^{\mathrm{Q}} (6 - 5h\kappa_1) \end{pmatrix}. \tag{B.10}$$

C. Alternative Form of the Generalized Constitutive Equations

In this section, a method to obtain the alternative form (47) of the two generalized constitutive equations (46) is shown.

The constitutive equation

$$\widetilde{\mathbf{d}} = \mathbf{D}\widetilde{\mathbf{Q}} + \mathbf{D}^+\widetilde{\boldsymbol{\tau}}^+ + \mathbf{D}^-\widetilde{\boldsymbol{\tau}}^- \tag{C.1}$$

is transformed directly by multiplying it by the shearing stiffness matrix $\mathbf{L}$ (it is the inverse of the shearing compliance matrix $\mathbf{D}$) and one obtains

$$\widetilde{\mathbf{Q}} = \mathbf{L}\widetilde{\mathbf{d}} + \mathbf{L}^+\widetilde{\boldsymbol{\tau}}^+ + \mathbf{L}^-\widetilde{\boldsymbol{\tau}}^- \tag{C.2}$$

where $\mathbf{L}^+ = -\mathbf{L}\mathbf{D}^+$ and $\mathbf{L}^- = -\mathbf{L}\mathbf{D}^-$.

For the other constitutive equation:

$$\boldsymbol{\epsilon} = \mathbf{C}\mathbf{q} + \sigma^+\mathbf{c}^+ + \sigma^-\mathbf{c}^- + f_3\mathbf{c^3}, \tag{C.3}$$

the task is more complicated because the compliance matrix $\mathbf{C}$ is not invertible. Its fourth and eighth columns are linear combinations of the third and seventh columns. This is due to the fact that N_{21} and M_{21} are linearly dependent of N_{12} and M_{12} as shown in (21). Matrix operations allow obtaining the alternative form of the generalized constitutive equation

$$\mathbf{q} = \mathbf{K}\boldsymbol{\epsilon} + \sigma^+\mathbf{k}^+ + \sigma^-\mathbf{k}^- + f_3\mathbf{k^3}, \tag{C.4}$$

where the stiffness matrix $\mathbf{K}$ and vectors $\mathbf{k}^+$, $\mathbf{k}^-$, and $\mathbf{k^3}$ are defined by

$$\begin{aligned} \mathbf{K} &= \mathbf{H^2}\left(\mathbf{H^1 C H^2}\right)^{-1}\mathbf{H^1} \\ \mathbf{k}^+ &= -\mathbf{K}\mathbf{c}^+, \\ \mathbf{k}^- &= -\mathbf{K}\mathbf{c}^-, \\ \text{and } \mathbf{k^3} &= -\mathbf{K}\mathbf{c^3}. \end{aligned} \tag{C.5}$$

In the previous definition, the components of matrices $\mathbf{H^1}$ and $\mathbf{H^2}$ are

$$\mathbf{H^1} = \begin{pmatrix} 1 & 0 & 0 & 0 & 0 & 0 & 0 & 0 \\ 0 & 1 & 0 & 0 & 0 & 0 & 0 & 0 \\ 0 & 0 & 1 & 1 & 0 & 0 & 0 & 0 \\ 0 & 0 & 0 & 0 & 1 & 0 & 0 & 0 \\ 0 & 0 & 0 & 0 & 0 & 1 & 0 & 0 \\ 0 & 0 & 0 & 0 & 0 & 0 & 1 & 1 \end{pmatrix} \tag{C.6}$$

and

$$\mathbf{H^2} = \begin{pmatrix} 1 & 0 & 0 & 0 & 0 & 0 \\ 0 & 1 & 0 & 0 & 0 & 0 \\ 0 & 0 & 1 & 0 & 0 & 0 \\ 0 & 0 & 1 & 0 & 0 & \delta\kappa \\ 0 & 0 & 0 & 1 & 0 & 0 \\ 0 & 0 & 0 & 0 & 1 & 0 \\ 0 & 0 & 0 & 0 & 0 & 1 \\ 0 & 0 & \frac{h^2}{12}\delta\kappa & 0 & 0 & 1 \end{pmatrix}. \tag{C.7}$$

One can verify that with these matrices, (21) and the supplementary "equilibrium" equation (36) included in Sanders model [14] are satisfied.

Data Availability

The equations used to support the findings of this study are included within the article.

Conflicts of Interest

The authors declare that they have no conflicts of interest.

References

[1] N. J. Pagano, "Stress fields in composite laminates," *International Journal of Solids and Structures*, vol. 14, no. 5, pp. 385–400, 1978.

[2] A. E. H. Love, "Philosophical transactions of the royal society of london," *Mathematical, Physical & Engineering Sciences*, vol. 179, Article ID 491546, pp. 491–546, 1888.

[3] R. D. Mindlin, "Influence of rotatory inertia and shear on flexural motions of isotropic elastic plates," *Journal of Applied Mechanics*, vol. 18, pp. 31–36, 1951.

[4] E. Reissner, "The effect of transverse shear deformation on the bending of elastic plates," *Journal of Applied Mechanics*, pp. 69–77, 1945.

[5] J. N. Reddy, "A simple higher-order theory for laminated composite plates," *Journal of Applied Mechanics*, vol. 51, no. 4, pp. 745–752, 1984.

[6] E. Carrera, "Historical review of Zig-Zag theories for multilayered plates and shells," *Applied Mechanics Reviews*, vol. 56, no. 3, pp. 287–308, 2003.

[7] A. Lebée and K. Sab, "A Bending-Gradient model for thick plates. Part I: Theory," *International Journal of Solids and Structures*, vol. 48, no. 20, pp. 2878–2888, 2011.

[8] A. Lebée and K. Sab, "On the generalization of Reissner plate theory to laminated plates, Part I: Theory," *Journal of Elasticity: The Physical and Mathematical Science of Solids*, vol. 126, no. 1, pp. 39–66, 2017.

[9] E. Carrera, "Theories and finite elements for multilayered, anisotropic, composite plates and shells," *Archives of Computational Methods in Engineering: State-of-the-Art Reviews*, vol. 9, no. 2, pp. 87–140, 2002.

[10] E. Reissner, "Free boundaries and jets in the theory of cavitation," *Journal of Mathematics and Physics*, vol. 29, pp. 90–95, 1950.

[11] A. Chabot, *Analyse des efforts à linterface entre les couches des matériaux composites à laide de modèles multiparticulaires de matériaux multicouches (M4). [Ph.D. thesis]*, Ecole Nationale des Ponts et Chaussées, 1997.

[12] R. P. Carreira, J. F. Caron, and A. Diaz Diaz, "Model of multilayered materials for interface stresses estimation and validation by finite element calculations," *Mechanics of Materials*, vol. 34, no. 4, pp. 217–230, 2002.

[13] R. Alvarez-Lima, A. Diaz-Diaz, J.-F. Caron, and S. Chataigner, "Enhanced layerwise model for laminates with imperfect interfaces - Part 1: Equations and theoretical validation," *Composite Structures*, vol. 94, no. 5, pp. 1694–1702, 2012.

[14] J. L. Sanders Jr, "An improved first-approximation theory for thin shells," Tech. Rep. NASA TR-R24, United States Government Publishing Office, Washington, DC, USA, 1959.

[15] W. Flügge, *Stresses in Shells*, Springler-Verlag, 1966.

[16] E. Ventsel and T. Krauthammer, *Thin Plates and Shells: Theory, Analysis and Applications*, Marcel Dekker, New York, NY, USA, 2001.

[17] V. Z. Vlasov, "NASA-TT-F," Tech. Rep., National Aeronautics and Space Administration, 1964.

[18] P. M. Naghdi, *In Linear Theories of Elasticity and Thermoelasticity*, Springer, 1973.

[19] J. N. Reddy, *Theory and Analysis of Elastic Plates and Shells*, CRC Press, 2nd edition, 2006.

[20] M. H. Toorani and A. A. Lakis, "General equations of anisotropic plates and shells including transverse shear deformations, rotary inertia and initial curvature effects," *Journal of Sound and Vibration*, vol. 237, no. 4, pp. 561–615, 2000.

[21] M. H. Toorani and A. A. Lakis, "Free vibrations of non-uniform composite cylindrical shells," *Nuclear Engineering and Design*, vol. 236, no. 17, pp. 1748–1758, 2006.

[22] D. D. Fox, "Transverse shear and normal stresses in nonlinear shell theory," *Computers & Structures*, vol. 75, no. 3, pp. 313–319, 2000.

[23] F. Tornabene and E. Viola, "Static analysis of functionally graded doubly-curved shells and panels of revolution," *Meccanica*, vol. 48, no. 4, pp. 901–930, 2013.

[24] E. Viola, F. Tornabene, and N. Fantuzzi, "Static analysis of completely doubly-curved laminated shells and panels using general higher-order shear deformation theories," *Composite Structures*, vol. 101, pp. 59–93, 2013.

[25] E. Trefftz, "Ableitung der Schalenbiegungsgleichungen mit dem Castiglianoschen Prinzip," *ZAMM - Journal of Applied Mathematics and Mechanics/Zeitschrift für Angewandte Mathematik und Mechanik*, vol. 15, no. 1-2, pp. 101–108, 1935.

[26] J. L. Synge and W. Z. Chien, "The intrinsic theory of elastic shells and plates," *Von KÃirmÃin Anniversary Volume*, Article ID 103120, pp. 103–120, 1941.

[27] W.-Z. Chien, "The intrinsic theory of thin shells and plates. I. General theory," *Quarterly of Applied Mathematics*, vol. 1, pp. 297–327, 1944.

[28] Y.-G. Fang, J.-H. Pan, and W.-X. Chen, "Theory of thick-walled shells and its application in cylindrical shell," *Applied Mathematics and Mechanics-English Edition*, vol. 13, no. 11, pp. 1055–1065, 1992.

[29] G. Z. Voyiadjis and G. Shi, "A refined two-dimensional theory for thick cylindrical shells," *International Journal of Solids and Structures*, vol. 27, no. 3, pp. 261–282, 1991.

[30] G. Z. Voyiadjis and P. Woelke, "A refined theory for thick spherical shells," *International Journal of Solids and Structures*, vol. 41, no. 14, pp. 3747–3769, 2004.

[31] A. W. Leissa, "Scientific and Technical Information Office," Tech. Rep. NASA SP-160, National Aeronautics and Space Administration, Washington, DC, USA, 1969.

[32] A. W. Leissa, "Scientific and Technical Information Office," Tech. Rep. NASA SP-288, National Aeronautics and Space Administration, Washington, DC, USA, 1973.

[33] M. L. Bucalem and K. J. Bathe, "High-order MITC general shell elements," *International Journal for Numerical Methods in Engineering*, vol. 36, no. 21, pp. 3729–3754, 1993.

[34] P.-S. Lee and K.-J. Bathe, "The quadratic MITC plate and MITC shell elements in plate bending," *Advances in Engineering Software*, vol. 41, no. 5, pp. 712–728, 2010.

[35] A. Diaz Diaz, J.-F. Caron, and R. P. Carreira, "Software application for evaluating interfacial stresses in inelastic symmetrical laminates with free edges," *Composite Structures*, vol. 58, no. 2, pp. 195–208, 2002.

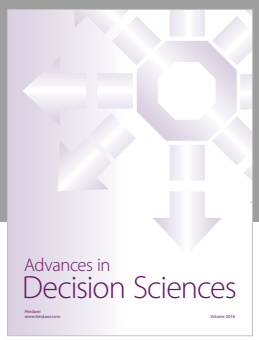

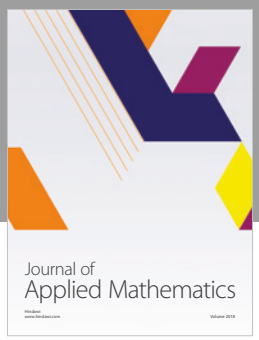

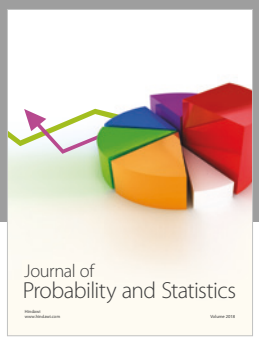

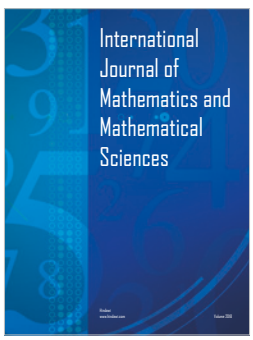

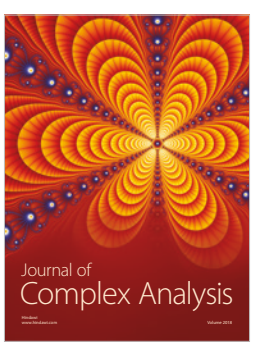

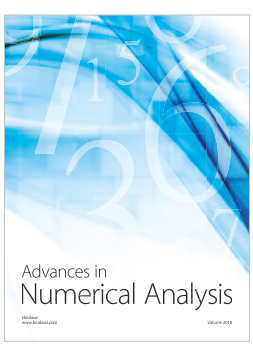

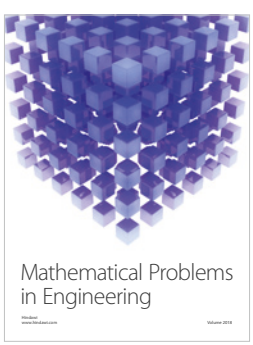

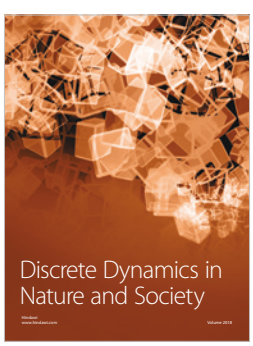

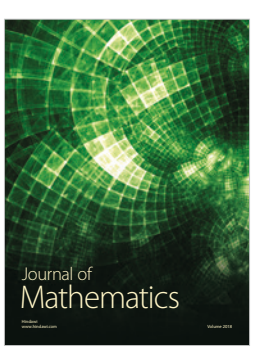

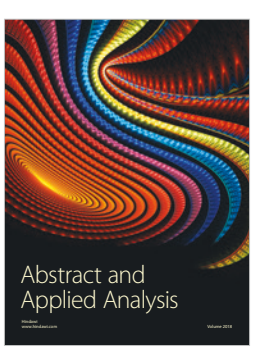

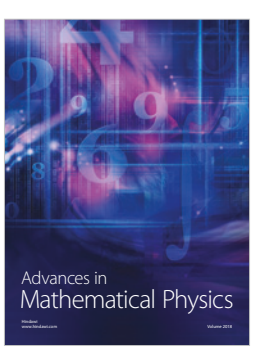

Hindawi

Submit your manuscripts at
www.hindawi.com